MATERIALS CHEMISTRY FRONTIERS

RESEARCH ARTICLE

View Article Online
View Journal | View Issue

Cite this: *Mater. Chem. Front.*, 2023, **7**, 1345

Vapochromic films of π-conjugated polymers based on coordination and desorption at hypervalent tin(IV)-fused azobenzene compounds†

Masayuki Gon, Yusuke Morisaki, Kazuya Tanimura, Kazuo Tanaka * and Yoshiki Chujo

Received 12th December 2022,
Accepted 31st January 2023

DOI: 10.1039/d2qm01295b

rsc.li/frontiers-materials

We report the synthesis and vapochromic behaviors of film materials consisting of hypervalent tin-containing π-conjugated polymers. We prepared copolymers with brominated tin-fused azobenzenes and modified fluorene having tetraethylene glycol as a side chain. The synthesized polymers showed good film-formability and high affinity with coordinating solvent molecules such as dimethyl sulfoxide (DMSO). In particular, we discovered distinct color changes from blue to purple when exposed to DMSO vapor. It was revealed that color changes should originate from reversible alteration of the coordination-number between five and six of hypervalent tin(IV) in the azobenzene compounds involved in the main-chain conjugation. Moreover, we also observed that binding constants between tin and coordinating solvents could be influenced by two substitutions on the tin atom and subsequently modulated responsivity of vapochromism in films by altering the type of substituent. Furthermore, the color-change behaviors can be estimated by quantum calculations with density functional theory. We demonstrate not only that hypervalent tin can work as a switching unit for modulating the electronic structures of π-conjugated polymers triggered by solvent coordination but also that vapochromic behaviors in films can be predicted by estimating the affinity between hypervalent tin and solvent molecules with theoretical calculations.

Introduction

Molecular detection without expensive instruments is a fundamental technology for constructing facile environmental assessments and daily health checking systems. To meet the demands for manufacturing practical sensors, organic materials are a versatile platform because of flexibility in material design which enables us to realize selective and sensitive detection for the targets by adjusting molecular structures.[1–3] In particular, π-conjugated polymers have attracted attention because of various advantages such as not only superior light-absorption and emission properties[4] but also good film-formability and printability in addition to designability.[5,6] Owing to such advantages, so far, various chemical sensors based on π-conjugated polymers have been developed.[7–10]

Vapochromism is known as the phenomenon in which color changes can be reversibly induced by vapor absorption and subsequently desorption.[11–13] In the absence of a direct connection between a chromophore and a target, vapochromic behaviors can be obtained. In the case of some kinds of crystalline samples, crystal–crystal transition can be induced by vapor fuming with specific solvents, followed by chromic behaviors.[14–23] Alterations of intramolecular structures and/or intermolecular distributions of chromophores including π-conjugated systems or transition metals should be responsible for optical changes in these materials. Optical changes can be recently realized in films consisting of π-conjugated polymers.[24,25] By vapor fuming, annealing processes should proceed. As a result, apparent and emission color changes that originated from morphology alterations of π-conjugated polymers can be observed. In these materials, dissolving into solvents and film-formation should be required for restoring the initial state.

If a connection can be formed between chromophores and the targets, sensitivity and selectivity can be improved. Indeed, in the case of metal complexes with organic ligands, chromic behaviors are also inducible by the direct coordination of solvent molecules to the metal centers of complexes with good sensitivity.[26–32] As a practical application, complex-doped polymer films have been also prepared.[33–38] Selectivity can be tuned by choosing the type of metal center that can coordinate with the

Department of Polymer Chemistry, Graduate School of Engineering, Kyoto University Katsura, Nishikyo-ku, Kyoto 615-8510, Japan.
E-mail: tanaka@poly.synchem.kyoto-u.ac.jp

† Electronic supplementary information (ESI) available. See DOI: https://doi.org/10.1039/d2qm01295b

target. However, vapochromism from film materials with main-chain-type π-conjugated polymers consisting of metal complexes could be hardly accomplished. Although organoboron complex-containing polymers can exhibit optical changes by reacting with fluoride anions, reversible responses were principally impossible due to the extremely high stability of the B–F bond.[39–43] Furthermore, anion sensors can work only in solution.[44] Besides anions, the partially reversible sensors for neutral donor molecules such as pyridine in solution were also prepared.[45] Although the vapochromic film was developed with the interaction between poly(9-borafluorene) and NH_3 vapor,[46] the number of examples is limited. Therefore, the development of vapochromic film materials composed of main-chain-type π-conjugated polymers consisting of metal complexes is a next goal not only for demonstrating a new modulation method of electronic properties of highly expanded π-conjugated systems but also for obtaining property-adjustable film sensors in which various properties can be tuned according to the preprogrammed design.

Recently, we proposed the design concept of heteroatom-containing polymers by employing "element-blocks", which are a minimum functional unit containing heteroatoms, to obtain novel functions originating from loaded elements.[47–49] Based on this concept, we have developed main-chain-type π-conjugated molecules and polymers with boron-fused azo (N═N) or azomethine (C═N) groups.[25,50–57] They showed various functions such as film-state visible to NIR emission,[25,51–54,57] stimuli-responsiveness,[25] aggregation-induced emission (AIE),[53,54,57,58] and crystallized-induced emission enhancement (CIEE).[51,52,59–63] Hypervalent compounds are a class of molecules in which over eight electrons are formally assigned around a valence shell of a main group element beyond the limit of the Lewis octet rule.[64–66] More recently, we reported that a series of hypervalent tin-fused azobenzene (TAz) compounds with five-coordinated distorted trigonal bipyramidal geometries.[67,68] They exhibited absorption and emission bands from the orange to the NIR region despite the fact that the small π-conjugated systems are involved in these molecules.[69] Some hypervalent compounds can change the coordination numbers of their atom centers upon the interaction between the Lewis acidic atom centers and Lewis basic substrates.[70–73] In our case, hypsochromic shifts of the spectra can be induced by solvent coordination to the tin center with the coordination-number change from five to six.[67] In the crystalline state, vapochromic behaviors were observed by encapsulation of dimethyl sulfoxide (DMSO) vapor with crystal–crystal transition. However, it is still difficult to apply the vapochromism of these compounds to practical sensing materials due to fragility of crystal powders. Moreover, crystal–crystal transitions followed by collapse of regular structures limited the reversibility of chromic behaviors.

Herein, we show the synthesis and unique properties of π-conjugated copolymers with TAz and fluorene moieties which can be a film-type vapochromic sensor. Two types of the TAz derivatives having methyl or phenyl groups at tin were prepared. In the fluorene units, tetraethylene glycol (TEG) side chains were introduced for improving the affinity of the hydrophobic π-conjugated polymers to highly polar coordinating solvents. Accordingly, the distinct color change from blue to purple was observed in films when exposed to DMSO vapor. We demonstrate here that molecular coordination at the hypervalent element in polymers can be a trigger for drastically changing the electronic structure of main-chain π-conjugation. Moreover, we were able to explain chromic behaviors with theoretical calculations. In particular, we proved that binding constants of solvent molecules can be estimated by the length of dative bonds between tin and coordinated atoms. We also showed that vapochromic behaviors are correlated with the affinity which can be evaluated with calculations.

Results and discussion

Synthesis and characterization

Scheme 1 shows the synthesis of the TAz compounds. The tridentate ligand of azobenzene (**1**) was prepared according to the literature.[57] Dehydration condensation was performed with **1** and diphenyltin(IV) oxide in acetone under reflux conditions to afford **TAzPh** in 59% isolated yield. **TAzMe** was obtained through the reaction with **1** and dimethyltin(IV) dichloride in the presence of sodium hydroxide in 74% isolated yield. The bromine groups in these TAz compounds were intended to be used for polymerization.

Next, we synthesized π-conjugated copolymers including the TAz moieties (Scheme 2). The modified fluorene compound having two TEG groups as side chains was designed as a comonomer to improve solubility in polar solvents, such as dimethyl sulfoxide (DMSO), dimethyl formamide (DMF), methanol (MeOH) and acetonitrile (MeCN), which have the potential to coordinate to the tin center. Trimethylstannyl groups were introduced through lithiation with **2** and subsequently addition of trimethyltin chloride, and the comonomer **3** was obtained in 95% isolated yield. Polymerization for preparing **P-TAzPh** and **P-TAzMe** was conducted *via* the Migita–Kosugi–Stille cross coupling reaction[74,75] with **TAzPh** or **TAzMe** and **3** in the presence of $Pd_2(dba)_3$ (dba = dibenzylideneacetone) and XPhos (2-dicyclohexylphosphino-2′,4′,6′-triisopropylbiphenyl), respectively. The products were purified and fractionated by high performance liquid chromatography (HPLC). The molecular weights were determined using gel permeation chromatography (GPC) with polystyrene standards. Consequently, we isolated **P-TAzPh** (17%, M_n = 5,200 (n = 6.9), PDI = 1.3, PDI: poly dispersity index) and **P-TAzMe** (25%, M_n = 6,200 (n = 9.7), PDI = 1.3). All products were characterized by ^{1}H, ^{13}C and ^{119}Sn NMR spectroscopy,

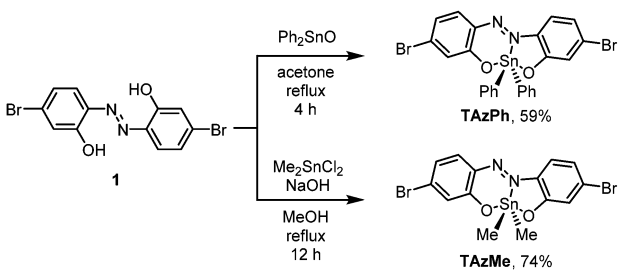

Scheme 1 Synthesis of TAz monomers.

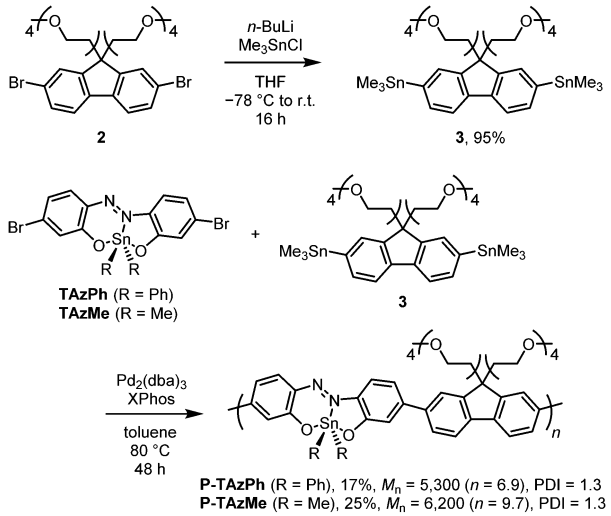

Scheme 2 Synthesis of TAz polymers.

high-resolution mass spectrometry (HRMS) and elemental analyses (see the ESI†). These characterization data enabled us to investigate the properties of the TAz derivatives.

Optical properties in diluted solution

First, we investigated the fundamental optical properties of the TAz monomers and polymers by UV–vis absorption and photoluminescence (PL) measurements in toluene (1.0×10^{-5} M) (Fig. 1 and Table 1). **TAzPh** and **TAzMe** showed absorption bands at around 550 nm and emission with the peaks around 670 nm. These long absorption and emission bands were unique characteristics of the TAz derivatives originating from distorted trigonal bipyramidal geometry consisting of a three center–four electron (3c-4e) bond at apical positions and a sp^2 hybrid orbital at equatorial positions.[67] Both spectra showed bathochromic shifts after copolymerization with the fluorene units. The peak tops of absorption and emission bands reached 600 and 680 nm, respectively. In addition, the band shapes of the emission spectra were sharpened, and the absolute PL quantum yields (Φ_{PL}s) were improved. The enhancement of rigidity by the expansion of π-conjugation through the polymer main-chain could be responsible for emission improvement. The **TAzMe** derivatives had more efficient emission than **TAzPh** ones in the deep red region, implying that small alkyl chains on the tin center might contribute to the construction of planar π-conjugation system through polymer main-chains especially in the excited state.

We previously reported that solvent coordination to the tin center induced the coordination-number change from five to six followed by hypsochromic shifts of the absorption and emission bands.[67] To examine the optical properties of the TAz derivatives in the polymer main-chain, we compared the solvent effects on the optical properties of monomers and polymers and estimated the coordination-number change (Fig. 1 and Fig. S1, ESI,† Table 1). In the case of non-coordinating solvents such as toluene and chloroform ($CHCl_3$), spectrum shifts were hardly

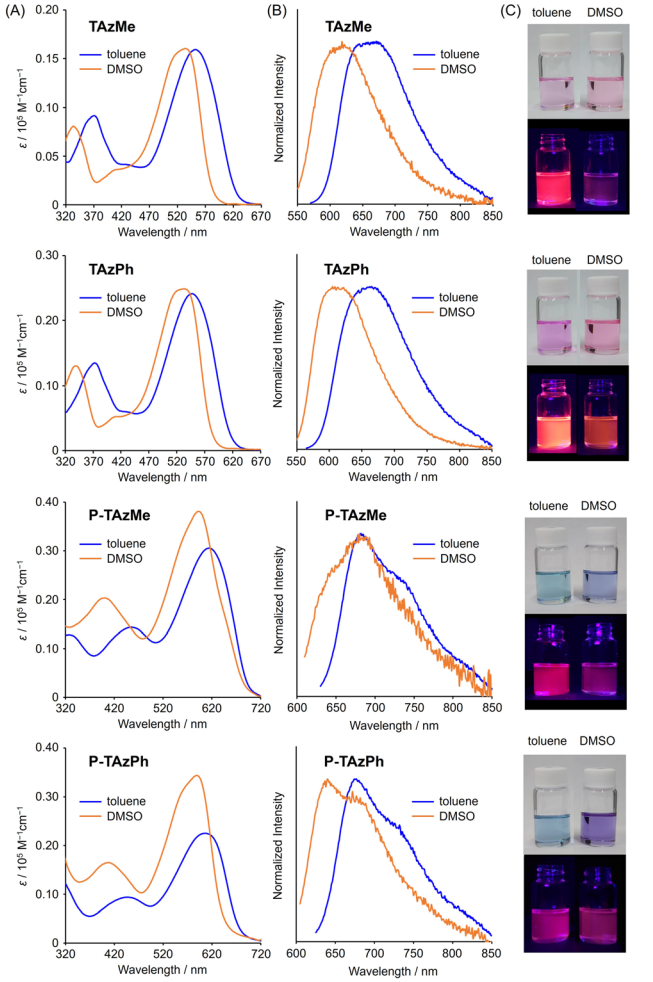

Fig. 1 (A) UV–vis absorption and (B) PL spectra of **TAzMe**, **TAzPh**, **P-TAzMe** and **P-TAzPh** (1.0×10^{-5} M for monomers and 1.0×10^{-5} M per repeating unit for polymers) in toluene (blue line) and toluene/DMSO = 1/99 v/v (orange line). (C) Photographs under room light (upper) and irradiated by 365 nm (below).

Table 1 Spectroscopic data of TAz derivatives in diluted solution (1.0×10^{-5} M)

	Solvent	λ_{abs}/nm	λ_{PL}[b]/nm	Φ_{PL}[bc]/%
TAzMe	Toluene	552	671	18.0
	DMSO [a]	534	618	1.3
TAzPh	Toluene	547	665	15.6
	DMSO [a]	533	605	3.7
P-TAzMe	Toluene	614	682	24.4
	DMSO [a]	593	680	1.0
P-TAzPh	Toluene	606	677	19.2
	DMSO [a]	583	640	2.2

[a] In mixed solvent, toluene/DMSO = 1/99 v/v. [b] Excited at λ_{abs}. [c] Absolute PL quantum yield.

observed, while clear hypsochromic shifts were observed in coordinating solvents such as DMSO, DMF, MeOH and MeCN. Since similar changes in optical properties were induced both in monomers and polymers, we concluded that the solvent

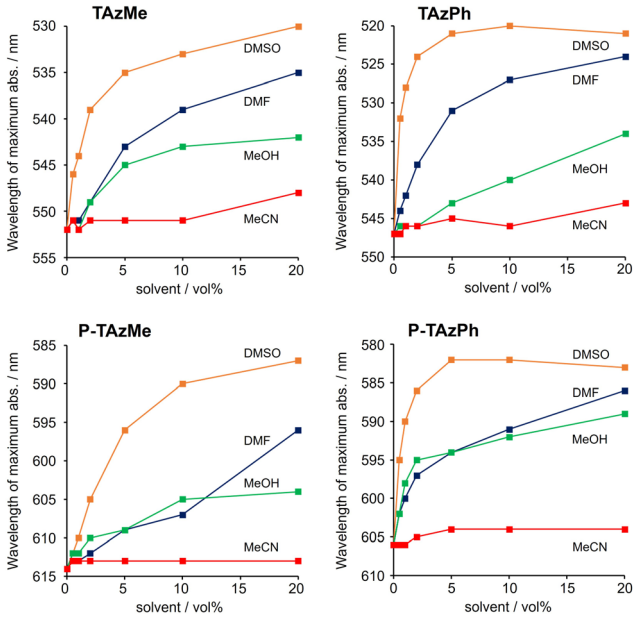

Fig. 2 Titration data of **TAzMe**, **TAzPh**, **P-TAzMe** and **P-TAzPh**. Hypsochromic shifts of wavelengths of maximum absorption depending on solvent vol% in toluene (1.0×10^{-5} M for monomers and 1.0×10^{-5} M per repeating unit for polymers). Full spectrum data are shown in the ESI.†

coordination was able to proceed at the hypervalent tin compounds in the polymer main-chains. Moreover, the degree of the peak shift, which represents strength of binding, was significantly dependent on the type of solvents. Fig. 2 shows relationships with wavelengths of maximum absorption by increasing the ratio of the coordinating solvents from 0 to 20 vol% in toluene. Full titration data from 0 to 99 vol% are shown in Fig. S2–S7 and Tables S1–S4 (ESI†). Accordingly, the solvent coordination to the tin center was stronger in the following order: DMSO > DMF > MeOH > MeCN. Additionally, it was shown that the **TAzPh** derivatives showed larger shifts than **TAzMe** ones judging from width of the hypsochromic shifts. To get more insight into the coordination, we estimated a binding constant (K) with a curve fitting method based on 1 to 1 coordination according to our previous work (Table 2 and Fig. S8, ESI†).[67] It was shown that the K values were larger in the following order; DMSO > DMF ≫ (MeOH and MeCN, too weak to obtain reliable values). Furthermore, the K value of **TAzPh** was larger than that of **TAzMe**. This should be because that a methyl group has stronger electron-donating ability than a phenyl group and it reduces the Lewis acidity of tin. In addition, lower Φ_{PL} values were observed from the stronger-coordinated compounds (Fig. S6 and S7, ESI†). Structural distortion followed by enhancement of nonradiative decay should be caused by the solvent coordination.[67] It should be noted that

Table 2 Binding constants of TAz monomers in various solvents[a]

	K_{DMSO}/M^{-1}	K_{DMF}/M^{-1}
TAzMe	2.7	0.59
TAzPh	11	1.3

[a] Determined in toluene at room temperature (25 °C).

the polymers showed similar solvent effects. In other words, solvent coordination to the TAz moieties should occur in the polymers. In **P-TAzMe**, a complete hypsochromic shift in the PL spectrum was not observed in toluene/DMSO = 1/99 v/v (Fig. 1B). This indicates that the solvent coordination can be controlled by the substituents on the tin center.

Optical properties in polymer thin films

Next, we explored vapochromism in polymer films. We prepared thin films of **P-TAzPh** and **P-TAzMe** on quartz substrates (0.9 cm × 5.0 cm) using a spin-coating method (1000 rpm, 30 s, 100 μL of $CHCl_3$ solution (2 mg/300 μL)) and subsequently dried *in vacuo* for 12 h. We evaluated color changes and especially focused on their reversibility with the films by monitoring UV–vis absorption measurements with the exposure to DMSO, DMF, MeOH and CH_3CN vapors for 30 min and following dry with a hair dryer for 30 min at room temperature (Fig. 3 and Fig. S9, S10, ESI†). Accordingly, the most drastic color change and the recovery were found in the combination of **P-TAzPh** and DMSO vapor (Fig. 3B and D), and almost all other pairs were inactive (Fig. 3A and Fig. S10, ESI†). It should be noted that **P-TAzPh** showed repeatability of at least two cycles (Fig. 3C). If color changes are induced by morphology alteration and/or degradation of hypervalent tin compounds, it should be impossible to observe reversible behaviors. Thus, it can be said that coordination and desorption of solvent vapor at the hypervalent tin should be responsible for the vapochromic properties in the polymer film.

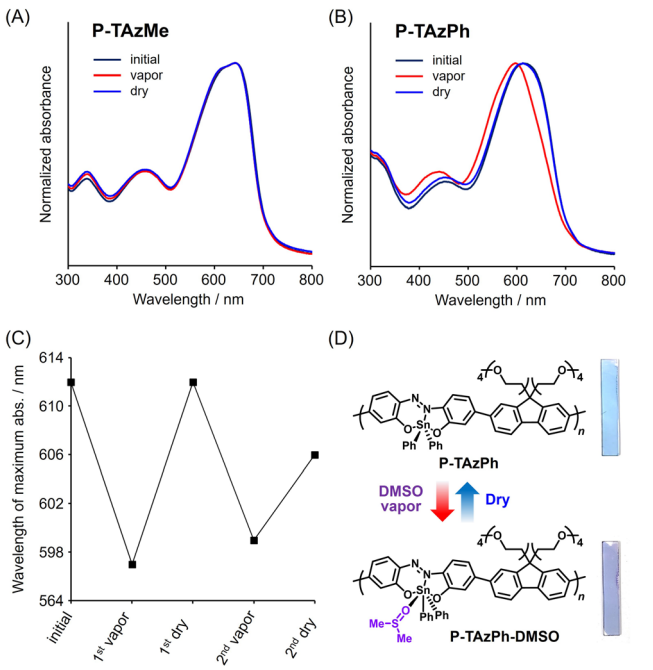

Fig. 3 UV–vis absorption spectra of (A) **P-TAzMe** and (B) **P-TAzPh** in the film before and after solvent annealing for 30 min, and recovery test by drying the film for 30 min at room temperature. (C) Reversible controls of the UV–vis absorption properties of **P-TAzPh** with exposure to DMSO vapor (30 min) and dry (30 min) processes at room temperature. (D) Illustration of plausible mechanism of vapochromism in the film with photographs under room light.

Since the vapochromic behaviors should be dependent on the magnitude of the binding constant, it is likely that the pair of **TAzPh** and DMSO showed the largest degree of optical changes.[67] Crystal–crystal transition was essential for presenting color changes with small molecules according to the previous work.[67] It should be emphasized that we succeeded in realizing vapochromism with polymer films which are easily applied to stimuli-responsive materials manufactured by a printing method. It should be noted that reversible color change was also detectable using DMF vapor, which was not observed from the crystalline sample in which it was dissolved by DMF vapor.[67] Interestingly, the **P-TAzMe** was inactive by exposure to DMSO vapor despite the fact that K_{DMSO} of **TAzMe** is larger than K_{DMF} of **TAzPh**. It is implied that bulky substituents around tin might make cavities which are capable of capturing solvent molecules. As a result, **P-TAzPh** can show higher sensitivity toward vapor fuming. In contrast to absorption spectra, the changes in PL spectra were hardly observed upon exposure to various solvent vapors regardless of non-coordinating or coordinating ones. (Fig. S11, ESI†). It might be because of intra- and intermolecular energy migration from DMSO coordinated sites to luminescent sites in film. By combining these results of absorption and emission behaviors in film, it is supported that the color change in absorption should be caused not by the solvent-vapor annealing process but by the solvent coordination to the tin center. Basically, strong concentration quenching occurred (Φ_{PL} = 3.4% for **P-TAzMe** and Φ_{PL} = 0.3% for **P-TAzPh**), and the value was almost similar before and after DMSO addition (Φ_{PL} = 3.2% for **P-TAzMe** and Φ_{PL} = 0.3% for **P-TAzPh** with DMSO vapor). It was hard to observe the luminescence behavior by the naked eye because the emission band reached the NIR area.

Theoretical calculations

We carried out quantum calculations with density functional theory (DFT) and time-dependent (TD)-DFT to simulate optical behaviors of the TAz derivatives with DMSO coordination. **M-TAzMe** and **M-TAzPh** which have fluorene units at both sides of **TAzMe** and **TAzPh**, respectively, were used as model compounds of the polymers for saving calculation costs. Accordingly, **TAzMe** exhibited a slightly longer absorption band (509 nm) than **TAzPh** (501 nm), and that behavior was qualitatively in good agreement with experimental data (Fig. S12B, ESI†). It was observed that the methyl groups can have an electron-donating ability because the HOMO (highest occupied molecular orbital) and LUMO (lowest unoccupied molecular orbital) energy levels of **TAzMe** were elevated compared to those of **TAzPh** (Fig. S12A, ESI†). Their DMSO adducts, **TAzMe-DMSO** and **TAzPh-DMSO**, showed larger energy gaps (475 and 469 nm, respectively) due to

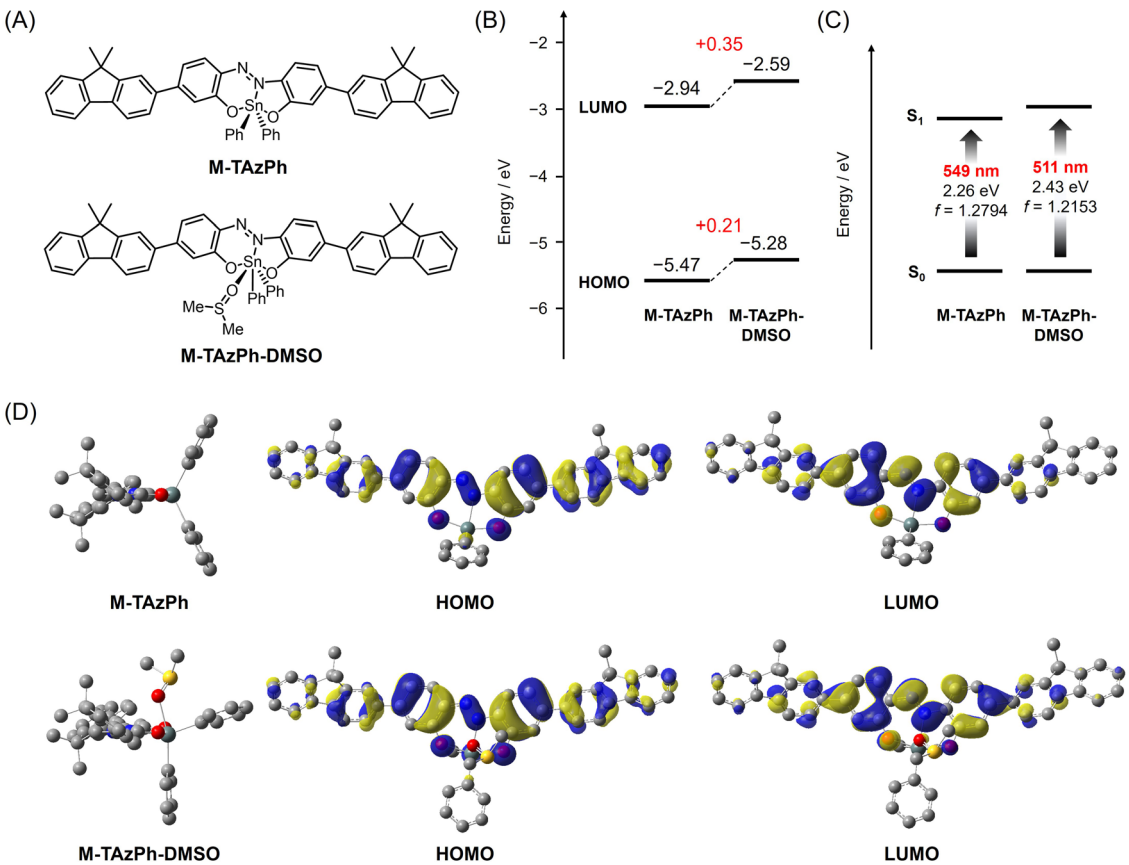

Fig. 4 Calculation results of **M-TAzPh** and **M-TAzPh-DMSO** as a model compound of **P-TAzPh** and its DMSO adduct, respectively, with DFT. (A) Chemical structures. (B) Calculated HOMO and LUMO energy levels, and (C) calculated $S_0 \rightarrow S_1$ transition bands and oscillator strengths (*f*). (D) Side view of optimized structures, and selected Kohn–Sham orbitals (isovalue = 0.02). Calculation details are shown in the ESI.†

the larger degree of elevation of the energy levels of the LUMO than the HOMO (Fig. S12, ESI†) with keeping molecular orbital (MO) shapes (Fig. S13, ESI†). Our previous research suggested that the hypsochromic shift and different effects on MO energy levels can be caused by coordination-number change of the hypervalent compound from five to six.[67] Concretely, elevation of LUMO and HOMO energy levels should be induced by the coordination of the oxygen lone pair in DMSO, which weakened the Sn–N coordination and enhanced electron-donating ability of oxygens at the apical positions of the ligand in the 3c-4e bond.

The hypsochromic shift induced by DMSO coordination was also effective in **M-TAzMe** and **M-TAzPh** (Fig. 4 and Fig. S12, ESI†). Similarly to the monomers, the shapes of MOs were preserved before and after DMSO coordination. These results are of significance for presenting distinct chromic behaviors because slight shape changes of MOs can secure large oscillator strength (f) associated with the value of a molar extinction coefficient (Fig. S14, ESI†). We previously reported that the binding constants of **TAzPh** derivatives can be estimated by the equation of $d = -0.0049 \times (\ln K_{DMSO}) + 2.3564$ (d: Sn–O (DMSO) bond length (Å) from an optimized structure).[67] According to this equation, we can estimate the binding constants as K_{DMSO} = 11.6 for **TAzPh** and 2.8 for **M-TAzPh** (Fig. S15, ESI†). The former value was well matched to the experimental data in this study (K_{DMSO} = 11 for **TAzPh**). Although **M-TAzPh** was not synthesized and the K value of **P-TAzPh** was difficult to experimentally estimate due to weak affinity, we can assume that the affinity to DMSO of **M-TAzPh** should be weaker than that of **TAzPh**. These calculation results support that DMSO coordination can induce hypsochromic color changes in the polymer thin film.

Conclusions

π-Conjugated copolymers composed of TAz and fluorene moieties with TEG side chains were synthesized. The substituents at the tin center play a critical role in solvent coordination. Indeed, phenyl groups had larger binding constants than methyl groups. As a result, we achieved observing clear vapochromism in thin films of the copolymer including **TAzPh** by fuming DMSO vapor, which was the pair having the largest binding constant. The hypsochromic shifts induced by solvent coordination both in solution and film were attributed to the coordination-number change of tin from five to six. This fact clearly indicates that the hypervalent tin atom can work as a switch module for modulating the electronic properties of π-conjugated polymers by employing the azobenzene ligand. Furthermore, the spectrum shift was supported by theoretical calculation. In particular, the binding constant was well predicted by the Sn–O (DMSO) bond length. This means that the binding constant and subsequently sensitivity in vapochromic behaviors in films could be estimated with the theoretical calculations on the basis of our estimation protocols described here. The studies are expected to be used for developing stimuli-responsive materials with inherent element properties.

Conflicts of interest

There are no conflicts to declare.

Acknowledgements

This work was partially supported by the Fujimori Science and Technology Foundation (for M. G.), and a Grant-in-Aid for Early-Career Scientists (for M. G.) (JP20K15334), for Scientific Research (B) (for M. G.) (JP22H02130), for Scientific Research (B) (for K. T.) (21H02001), for Exploratory Research (for K. T.) (JP21K19002), and for Scientific Research on Innovative Areas "New Polymeric Materials Based on Element-Blocks (No. 2401)" (JP24102013).

References

1 R. M. Crooks and A. J. Ricco, New Organic Materials Suitable for Use in Chemical Sensor Arrays, *Acc. Chem. Res.*, 1998, **31**, 219–227.
2 W. Al Zoubi and N. D. Al Mohanna, Membrane sensors based on Schiff bases as chelating ionophores – A review, *Spectrochim. Acta, Part A*, 2014, **132**, 854–870.
3 D. James, S. M. Scott, Z. Ali and W. T. O'Hare, Chemical Sensors for Electronic Nose Systems, *Microchim. Acta*, 2005, **149**, 1–17.
4 P. Kumar, A. Ghosh and D. A. Jose, Chemical Sensors for Water Detection in Organic Solvents and their Applications, *ChemistrySelect*, 2021, **6**, 820–842.
5 B. Li, S. Santhanam, L. Schultz, M. Jeffries-EL, M. C. Iovu, G. Sauvé, J. Cooper, R. Zhang, J. C. Revelli, A. G. Kusne, J. L. Snyder, T. Kowalewski, L. E. Weiss, R. D. McCullough, G. K. Fedder and D. N. Lambeth, Inkjet printed chemical sensor array based on polythiophene conductive polymers, *Sens. Actuators, B*, 2007, **123**, 651–660.
6 D. Khim, G.-S. Ryu, W.-T. Park, H. Kim, M. Lee and Y.-Y. Noh, Precisely Controlled Ultrathin Conjugated Polymer Films for Large Area Transparent Transistors and Highly Sensitive Chemical Sensors, *Adv. Mater.*, 2016, **28**, 2752–2759.
7 P. Minei and A. Pucci, Fluorescent vapochromism in synthetic polymers, *Polym. Int.*, 2016, **65**, 609–620.
8 S. W. Thomas, G. D. Joly and T. M. Swager, Chemical Sensors Based on Amplifying Fluorescent Conjugated Polymers, *Chem. Rev.*, 2007, **107**, 1339–1386.
9 J.-S. Yang and T. M. Swager, Fluorescent Porous Polymer Films as TNT Chemosensors: Electronic and Structural Effects, *J. Am. Chem. Soc.*, 1998, **120**, 11864–11873.
10 S. W. Thomas III, J. P. Amara, R. E. Bjork and T. M. Swager, Amplifying fluorescent polymer sensors for the explosives taggant 2,3-dimethyl-2,3-dinitrobutane (DMNB), *Chem. Commun.*, 2005, 4572–4574.
11 O. S. Wenger, Vapochromism in Organometallic and Coordination Complexes: Chemical Sensors for Volatile Organic Compounds, *Chem. Rev.*, 2013, **113**, 3686–3733.
12 X. Zhang, B. Li, Z.-H. Chen and Z.-N. Chen, Luminescence vapochromism in solid materials based on metal complexes

for detection of volatile organic compounds (VOCs), *J. Mater. Chem.*, 2012, **22**, 11427–11441.

13 E. Li, K. Jie, M. Liu, X. Sheng, W. Zhu and F. Huang, Vapochromic crystals: understanding vapochromism from the perspective of crystal engineering, *Chem. Soc. Rev.*, 2020, **49**, 1517–1544.

14 A. Kobayashi, Y. Fukuzawa and H.-C. Vapor-Controlled, Linkage Isomerization of a Vapochromic Bis(thiocyanato) platinum(II) Complex: New External Stimuli To Control Isomerization Behavior. Chang and M. Kato, *Inorg. Chem.*, 2012, **51**, 7508–7519.

15 D. Saito, T. Galica, E. Nishibori, M. Yoshida, A. Kobayashi and M. Kato, Reversible and Stepwise Single-Crystal-to-Single-Crystal Transformation of a Platinum(II) Complex with Vapochromic Luminescence, *Chem. – Eur. J.*, 2022, **28**, e202200703.

16 S. Yokoyama, H. Asahara and N. Nishiwaki, Vapochromic Properties of Diethenylpyrrole with Naphthyl Tethers Induced by Formation of a Distorted Structure in the Solid State, *Cryst. Growth Des.*, 2020, **20**, 1383–1387.

17 S. Ito, M. Yaegashi, K. Tanaka and Y. Chujo, Reversible Vapochromic Luminescence Accompanied by Planar Half-Chair Conformational Change of a Propeller-Shaped Boron β-Diketiminate Complex, *Chem. – Eur. J.*, 2021, **27**, 9194.

18 S. Ito, A. Hirose, M. Yamaguchi, K. Tanaka and Y. Chujo, Size-discrimination of volatile organic compounds utilizing gallium diiminate by luminescent chromism of crystallization-induced emission via encapsulation-triggered crystal–crystal transition, *J. Mater. Chem. C*, 2016, **4**, 5564–5571.

19 H. Sasaki, H. Imoto, T. Kitao, T. Uemura, T. Yumura and K. Naka, Fluorinated porous molecular crystals: vapor-triggered on–off switching of luminescence and porosity, *Chem. Commun.*, 2019, **55**, 6487–6490.

20 G. Xia, S. Shen, X.-M. Hu, Z. Jiang, K. Xu, M. Wang and H. Wang, Controlling Crystal Structures and Multiple Thermo- and Vapochromic Behaviors of Benzimidazole-Based Squaraine Dyes by Molecular Design and Solvent Adjustment, *Chem. – Eur. J.*, 2018, **24**, 13205–13212.

21 A. Sakon, A. Sekine and H. Uekusa, Powder Structure Analysis of Vapochromic Quinolone Antibacterial Agent Crystals, *Cryst. Growth Des.*, 2016, **16**, 4635–4645.

22 H. Naito, Y. Morisaki and Y. Chujo, *o*-Carborane-Based Anthracene: A Variety of Emission Behaviors, *Angew. Chem., Int. Ed.*, 2015, **54**, 5084–5087.

23 T. Panda, D. K. Maiti and M. K. Panda, Inkless Writing and Self-Erasing Security Feature of (*Z*)-1,2-Diarylacrylonitrile-Based Materials: A Confidential Data Communication, *ACS Appl. Mater. Interfaces*, 2018, **10**, 29100–29106.

24 S. Ito, M. Fukuyama, K. Tanaka and Y. Chujo, Effects of Regioregularity of π-Conjugated Polymers Composed of Boron β-Diketiminate on Their Stimuli-Responsive Luminescence, *Macromol. Chem. Phys.*, 2022, **223**, 2100504.

25 S. Ohtani, N. Yamada, M. Gon, K. Tanaka and Y. Chujo, The effect of alkyl chain lengths on the red-to-near-infrared emission of boron-fused azomethine conjugated polymers and their film-state stimuli-responsivities, *Polym. Chem.*, 2021, **12**, 2752–2759.

26 I. P. Oliveri, G. Malandrino, S. Mirabella and S. Di Bella, Vapochromic and chemiresistive characteristics of a nanostructured molecular material composed of a zinc(ii)-salophen complex, *Dalton Trans.*, 2018, **47**, 15977–15982.

27 Y. Soltani, S. J. Adams, J. Börger, L. C. Wilkins, P. D. Newman, S. J. A. Pope and R. L. Melen, Synthesis and photophysical properties of imine borane adducts towards vapochromic materials, *Dalton Trans.*, 2018, **47**, 12656–12660.

28 J. S. Ovens and D. B. Leznoff, Raman Detected Sensing of Volatile Organic Compounds by Vapochromic $Cu[AuX_2(CN)_2]_2$ (X = Cl, Br) Coordination Polymer Materials, *Chem. Mater.*, 2015, **27**, 1465–1478.

29 B. Orwat, M. J. Oh, M. Zaranek, M. Kubicki, R. Januszewski and I. Kownacki, Microwave-Accelerated C,N-Cyclometalation as a Route to Chloro-Bridged Iridium(III) Binuclear Precursors of Phosphorescent Materials: Optimization, Synthesis, and Studies of the Iridium(III) Dimer Behavior in Coordinating Solvents, *Inorg. Chem.*, 2020, **59**, 9163–9176.

30 H. Ohara, T. Ogawa, M. Yoshida, A. Kobayashi and M. Kato, Reversible luminescent colour changes of mononuclear copper(i) complexes based on ligand exchange reactions by N-heteroaromatic vapours, *Dalton Trans.*, 2017, **46**, 3755–3760.

31 E. J. Fernández, J. M. López-de-Luzuriaga, M. Monge, M. Montiel, M. E. Olmos, J. Pérez, A. Laguna, F. Mendizabal, A. A. Mohamed and J. P. Fackler, A Detailed Study of the Vapochromic Behavior of $\{Tl[Au(C_6Cl_5)_2]\}_n$, *Inorg. Chem.*, 2004, **43**, 3573–3581.

32 Y. Wu, X. Zhang, L.-J. Xu, M. Yang and Z.-N. Chen, Luminescent Vapochromism Due to a Change of the Ligand Field in a One-Dimensional Manganese(II) Coordination Polymer, *Inorg. Chem.*, 2018, **57**, 9175–9181.

33 G. Iasilli, F. Martini, P. Minei, G. Ruggeri and A. Pucci, Vapochromic features of new luminogens based on julolidine-containing styrene copolymers, *Faraday Discuss.*, 2017, **196**, 113–129.

34 M. Ahmad, I. Platonova, A. Battisti, P. Minei, G. Brancato and A. Pucci, Highly selective vapochromic fluorescence of polycarbonate films Doped with an ICT-Based solvatochromic probe, *J. Polym. Sci., Part B: Polym. Phys.*, 2017, **55**, 1171–1180.

35 I. Platonova, A. Branchi, M. Lessi, G. Ruggeri, F. Bellina and A. Pucci, Zn(II)-bisthienylethynylbipyridine complex: Preparation, characterization and vapochromic behaviour in polymer films, *Dyes Pigm.*, 2014, **110**, 249–255.

36 P. Minei, M. Koenig, A. Battisti, M. Ahmad, V. Barone, T. Torres, D. M. Guldi, G. Brancato, G. Bottari and A. Pucci, Reversible vapochromic response of polymer films doped with a highly emissive molecular rotor, *J. Mater. Chem. C*, 2014, **2**, 9224–9232.

37 J. R. Kumpfer, S. D. Taylor, W. B. Connick and S. J. Rowan, Vapochromic and mechanochromic films from square-planar platinum complexes in polymethacrylates, *J. Mater. Chem.*, 2012, **22**, 14196–14204.

38 J. W. Grate, L. K. Moore, D. E. Janzen, D. J. Veltkamp, S. Kaganove, S. M. Drew and K. R. Mann, Steplike Response

Behavior of a New Vapochromic Platinum Complex Observed with Simultaneous Acoustic Wave Sensor and Optical Reflectance Measurements, *Chem. Mater.*, 2002, **14**, 1058–1066.
39 H. Helten, Doping the Backbone of π-Conjugated Polymers with Tricoordinate Boron: Synthetic Strategies and Emerging Applications, *Chem. – Asian J.*, 2019, **14**, 919–935.
40 M. Miyata and Y. Chujo, π-Conjugated Organoboron Polymer as an Anion Sensor, *Polym. J.*, 2002, **34**, 967–969.
41 H. Li and F. Jäkle, Universal Scaffold for Fluorescent Conjugated Organoborane Polymers, *Angew. Chem., Int. Ed.*, 2009, **48**, 2313–2316.
42 K. Hu, Z. Zhang, J. Burke and Y. Qin, Boron ''Doped'' Polyacetylenes, *J. Am. Chem. Soc.*, 2017, **139**, 11004–11007.
43 A. Lik, S. Jenthra, L. Fritze, L. Müller, K.-N. Truong and H. Helten, From Monodisperse Thienyl- and Furylborane Oligomers to Polymers: Modulating the Optical Properties through the Hetarene Ratio, *Chem. – Eur. J.*, 2018, **24**, 11961–11972.
44 Y. Adachi, F. Arai, M. Sakabe and J. Ohshita, Effect of the conjugation pathway on the electronic structures of p–π* conjugated polymers with fused borepin units, *Polym. Chem.*, 2021, **12**, 3471–3477.
45 A. Sundararaman, M. Victor, R. Varughese and F. Jäkle, A Family of Main-Chain Polymeric Lewis Acids: Synthesis and Fluorescent Sensing Properties of Boron-Modified Polythiophenes, *J. Am. Chem. Soc.*, 2005, **127**, 13748–13749.
46 I. A. Adams and P. A. Rupar, A Poly(9-Borafluorene) Homopolymer: An Electron-Deficient Polyfluorene with ''Turn-On'' Fluorescence Sensing of NH_3 Vapor, *Macromol. Rapid Commun.*, 2015, **36**, 1336–1340.
47 Y. Chujo and K. Tanaka, New Polymeric Materials Based on Element-Blocks, *Bull. Chem. Soc. Jpn.*, 2015, **88**, 633–643.
48 M. Gon, K. Tanaka and Y. Chujo, Recent progress in the development of advanced element-block materials, *Polym. J.*, 2018, **50**, 109–126.
49 K. Tanaka and Y. Chujo, Modulation of the solid-state luminescent properties of conjugated polymers by changing the connecting points of flexible boron element blocks, *Polym. J.*, 2020, **52**, 555–566.
50 M. Gon, K. Tanaka and Y. Chujo, Discovery of Functional Luminescence Properties Based on Flexible and Bendable Boron-Fused Azomethine/Azobenzene Complexes with O,N,O-Type Tridentate Ligands, *Chem. Rec.*, 2021, **21**, 1358–1373.
51 S. Ohtani, M. Nakamura, M. Gon, K. Tanaka and Y. Chujo, Synthesis of fully-fused bisboron azomethine complexes and their conjugated polymers with solid-state near-infrared emission, *Chem. Commun.*, 2020, **56**, 6575–6578.
52 S. Ohtani, M. Gon, K. Tanaka and Y. Chujo, Construction of the Luminescent Donor–Acceptor Conjugated Systems Based on Boron-Fused Azomethine Acceptor, *Macromolecules*, 2019, **52**, 3387–3393.
53 M. Gon, J. Wakabayashi, M. Nakamura, K. Tanaka and Y. Chujo, Controlling Energy Gaps of π-Conjugated Polymers by Multi-Fluorinated Boron-Fused Azobenzene Acceptors for Highly Efficient Near-Infrared Emission, *Chem. – Asian J.*, 2021, **16**, 696–703.
54 M. Gon, J. Wakabayashi, M. Nakamura, K. Tanaka and Y. Chujo, Preparation of Near-Infrared Emissive π-Conjugated Polymer Films Based on Boron-Fused Azobenzene Complexes with Perpendicularly Protruded Aryl Substituents, *Macromol. Rapid Commun.*, 2021, **42**, 2000566.
55 J. Wakabayashi, M. Gon, K. Tanaka and Y. Chujo, Near-Infrared Absorptive and Emissive Poly(*p*-phenylene vinylene) Derivative Containing Azobenzene–Boron Complexes, *Macromolecules*, 2020, **53**, 4524–4532.
56 M. Gon, J. Wakabayashi, K. Tanaka and Y. Chujo, Unique Substitution Effect at 5,5′-Positions of Fused Azobenzene–Boron Complexes with a N = N π-Conjugated System, *Chem. – Asian J.*, 2019, **14**, 1837–1843.
57 M. Gon, K. Tanaka and Y. Chujo, A Highly Efficient Near-Infrared-Emissive Copolymer with a N = N Double-Bond π-Conjugated System Based on a Fused Azobenzene–Boron Complex, *Angew. Chem., Int. Ed.*, 2018, **57**, 6546–6551.
58 J. Luo, Z. Xie, J. W. Y. Lam, L. Cheng, H. Chen, C. Qiu, H. S. Kwok, X. Zhan, Y. Liu, D. Zhu and B. Z. Tang, Aggregation-induced emission of 1-methyl-1,2,3,4,5-pentaphenylsilole, *Chem. Commun.*, 2001, 1740–1741.
59 S. Ohtani, Y. Takeda, M. Gon, K. Tanaka and Y. Chujo, Facile strategy for obtaining luminescent polymorphs based on the chirality of a boron-fused azomethine complex, *Chem. Commun.*, 2020, **56**, 15305–15308.
60 S. Ohtani, M. Gon, K. Tanaka and Y. Chujo, The Design Strategy for an Aggregation- and Crystallization-Induced Emission-Active Molecule Based on the Introduction of Skeletal Distortion by Boron Complexation with a Tridentate Ligand, *Crystals*, 2020, **10**, 615.
61 S. Ohtani, M. Gon, K. Tanaka and Y. Chujo, A Flexible, Fused, Azomethine–Boron Complex: Thermochromic Luminescence and Thermosalient Behavior in Structural Transitions between Crystalline Polymorphs, *Chem. – Eur. J.*, 2017, **23**, 11827–11833.
62 M. Nakamura, M. Gon, S. Natsuda, Y. Tamai, H. Ohkita, K. Tanaka and Y. Chujo, Development of NIR emissive fully-fused bisboron complexes with π-conjugated systems including multiple azo groups, *Dalton Trans.*, 2022, **51**, 74–84.
63 Y. Dong, J. W. Y. Lam, A. Qin, Z. Li, J. Sun, H. H.-Y. Sung, I. D. Williams and B. Z. Tang, Switching the light emission of (4-biphenylyl)phenyldibenzofulvene by morphological modulation: crystallization-induced emission enhancement, *Chem. Commun.*, 2007, 40–42.
64 J. I. Musher, The Chemistry of Hypervalent Molecules, *Angew. Chem., Int. Ed. Engl.*, 1969, **8**, 54–68.
65 R. Gillespie and B. Silvi, The octet rule and hypervalence: two misunderstood concepts, *Coord. Chem. Rev.*, 2002, **233–234**, 53–62.
66 K.-y Akiba, Studies on hypervalent compounds and synthetic work using heteroaromatic cations, *Heteroatom Chem.*, 2011, **22**, 207–274.
67 M. Gon, K. Tanaka and Y. Chujo, Vapochromic Luminescent π-Conjugated Systems with Reversible Coordination-Number Control of Hypervalent Tin(IV)-Fused Azobenzene Complexes, *Chem. – Eur. J.*, 2021, **27**, 7561–7571.

68 M. Gon, K. Tanimura, M. Yaegashi, K. Tanaka and Y. Chujo, PPV-type π-conjugated polymers based on hypervalent tin(IV)-fused azobenzene complexes showing near-infrared absorption and emission, *Polym. J.*, 2021, **53**, 1241–1249.

69 K. E. Bessler, J. A. dos Santos, V. M. Deflon, S. de Souza Lemos and E. Niquet, Organotin Dyes: Synthesis and Structural Characterization of Dibutyltin and Dimethyltin Complexes with 2,2′-Dihydroxyazobenzene, *Z. Anorg. Allg. Chem.*, 2004, **630**, 742–745.

70 C. Chuit, R. J. P. Corriu, C. Reye and J. C. Young, Reactivity of penta- and hexacoordinate silicon compounds and their role as reaction intermediates, *Chem. Rev.*, 1993, **93**, 1371–1448.

71 S. Yamaguchi, S. Akiyama and K. Tamao, Photophysical Properties Changes Caused by Hypercoordination of Organosilicon Compounds: From Trianthrylfluorosilane to Trianthryldifluorosilicate, *J. Am. Chem. Soc.*, 2000, **122**, 6793–6794.

72 N. Singh, K. Kumar, N. Srivastav, R. Singh, V. Kaur, J. P. Jasinski and R. J. Butcher, Exploration of fluorescent organotin compounds of α-amino acid Schiff bases for the detection of organophosphorous chemical warfare agents: quantification of diethylchlorophosphate, *New J. Chem.*, 2018, **42**, 8756–8764.

73 M. H. Chisholm, E. E. Delbridge and J. C. Gallucci, Modeling the catalyst resting state in aryl tin(iv) polymerizations of lactide and estimating the relative rates of transamidation, transesterification and chain transfer, *New J. Chem.*, 2004, **28**, 145–152.

74 M. Kosugi, K. Sasazawa, Y. Shimizu and T. Migita, REACTIONS OF ALLYLTIN COMPOUNDS III. ALLYLATION OF AROMATIC HALIDES WITH ALLYLTRIBUTYLTIN IN THE PRESENCE OF TETRAKIS(TRIPHENYLPHOSPHINE)PALLADIUM(O), *Chem. Lett.*, 1977, 301–302.

75 D. Milstein and J. K. Stille, A general, selective, and facile method for ketone synthesis from acid chlorides and organotin compounds catalyzed by palladium, *J. Am. Chem. Soc.*, 1978, **100**, 3636–3638.

Supplementary Information

Vapochromic Films of π-Conjugated Polymers Based on Coordination and Desorption at Hypervalent Tin(IV)-Fused Azobenzene Compounds

Masayuki Gon, Yusuke Morisaki, Kazuya Tanimura, Kazuo Tanaka* and Yoshiki Chujo

Department of Polymer Chemistry, Graduate School of Engineering, Kyoto University Katsura, Nishikyo-ku, Kyoto 615-8510, Japan

E-mail: tanaka@poly.synchem.kyoto-u.ac.jp

Key words: tin; azobenzene; hypervalent compound; vapochromism; absorption and emission

Contents page

General

^{1}H, $^{13}C\{^{1}H\}$ and ^{119}Sn NMR spectra were recorded on JEOL AL400 and ECX400 instruments at 400, 100 and 149 MHz, respectively. Samples were analyzed in $CDCl_3$. The chemical shift values were expressed relative to Me_4Si for ^{1}H, $^{13}C\{^{1}H\}$ NMR as an internal standard in $CDCl_3$ and Me_4Sn for ^{119}Sn NMR as a capillary standard. High-resolution mass spectrometry (HRMS) was performed at the Technical Support Office (Department of Synthetic Chemistry and Biological Chemistry, Graduate School of Engineering, Kyoto University), and the HRMS spectra were obtained on a Thermo Fisher Scientific EXACTIVE spectrometer for electrospray ionization (ESI) and a Bruker Daltonics ultrafleXtreme for matrix assisted laser desorption ionization (MALDI). UV–vis spectra were recorded on a SHIMADZU UV-3600i Plus spectrophotometer, and samples were analyzed at room temperature. HORIBA JOBIN YVON Fluorolog-3 was used for PL spectra. Absolute photoluminescence quantum efficiency (Φ_{PL}) was recorded on a Hamamatsu Photonics Quantaurus-QY Plus C13534-01. HITACHI HD-1263 TURBO 1200 was used as hair dryer.

Materials

Commercially available compounds used without purification:

Diphenyltin(IV) oxide (Sigma-Aldrich Co. LLC.)

Dimethyltin(IV) dichloride (FUJIFILM Wako Pure Chemical Corporation)

NaOH (FUJIFILM Wako Pure Chemical Corporation)

n-Butyllithium, in *n*-hexane, 1.57 mol/L (Kanto Chemical Co., Inc.)

Trimethyltin Chloride (Tokyo Chemical Industry Co, Ltd.)

$Pd_2(dba)_3$ (dba = dibenzylideneacetone) (Tokyo Chemical Industry Co, Ltd.)

2-Dicyclohexylphosphino-2′,4′,6′-triisopropylbiphenyl (XPhos) (Strem Chemicals, Inc.)

Commercially available solvents:

Acetone (super dehydrated grade, FUJIFILM Wako Pure Chemical Corporation), MeOH (deoxidized grade, FUJIFILM Wako Pure Chemical Corporation), toluene (deoxidized grade, FUJIFILM Wako Pure Chemical Corporation) used without purification.

Tetrahydrofuran (super dehydrated grade, FUJIFILM Wako Pure Chemical Corporation) was purified by

passage through solvent purification columns under N_2 pressure.[1]

Compounds prepared as described in the literatures:

4,4′-Dibromo-2,2′-dihydroxyazobenzene (**1**)[2]

13,13′-(2,7-Dibromo-9*H*-fluoren-9-ylidene)bis[2,5,8,11-tetraoxatridecane] (**2**)[3,4]

Synthetic procedures and characterization

Synthesis of TAzPh

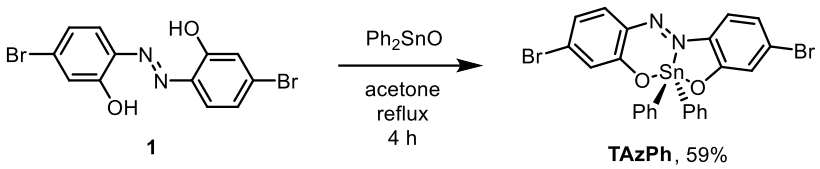

In a 50 mL round bottom flask, **1** (0.328 g, 0.88 mmol, 1 equiv.), diphenyltin(IV)oxide (0.382 g, 1.32 mmol, 1.5 equiv.) and 15 mL of acetone were added under N_2. Then, the solution was stirred at 60 °C for 4 h. After the reaction, the mixture was filtered to remove unreacted diphenyltin(IV) oxide, and the solvent was removed with a rotary evaporator to afford **TAzPh** (0.334 g, 0.520 mmol, 59%) as a violet crystal.

^{1}H NMR ($CDCl_3$, 400 MHz) δ 7.93–7.73 (m, $J_{H–Sn}$ = 39.9 Hz, 4H), 7.57 (d, J = 8.7 Hz, 1H), 7.44–7.42 (m, 7H), 7.31 (d, J = 2.2 Hz, 1H), 7.29 (d, J = 2.0 Hz, 1H), 7.01 (dd, J = 8.7, 2.1 Hz, 1H), 6.87 (dd, J = 8.8, 2.2 Hz, 1H) ppm. ^{13}C{^{1}H} NMR ($CDCl_3$, 400 MHz) δ 162.1, 160.9, 138.4, 136.5, 136.3, 136.2 ($J_{C–Sn}$ = 27.1 Hz), 136.2, 132.3, 130.9 ($J_{C–Sn}$ = 9.1 Hz), 129.3, 129.1 ($J_{C–Sn}$ = 43.6 Hz), 126.5, 123.2, 122.6, 121.8, 118.1 ppm. ^{119}Sn NMR ($CDCl_3$, 149 MHz) δ −364.1 ppm. HRMS (ESI) calcd. for $C_{24}H_{16}Br_2N_2O_2Sn$ $[M]^-$: 641.8580; found: 641.8575. Elemental analysis calcd. for $C_{24}H_{16}Br_2N_2O_2Sn$: C 44.84 H 2.51 N 4.36 Br 24.86, found: C 44.60 H 2.56 N 4.26 Br 24.63.

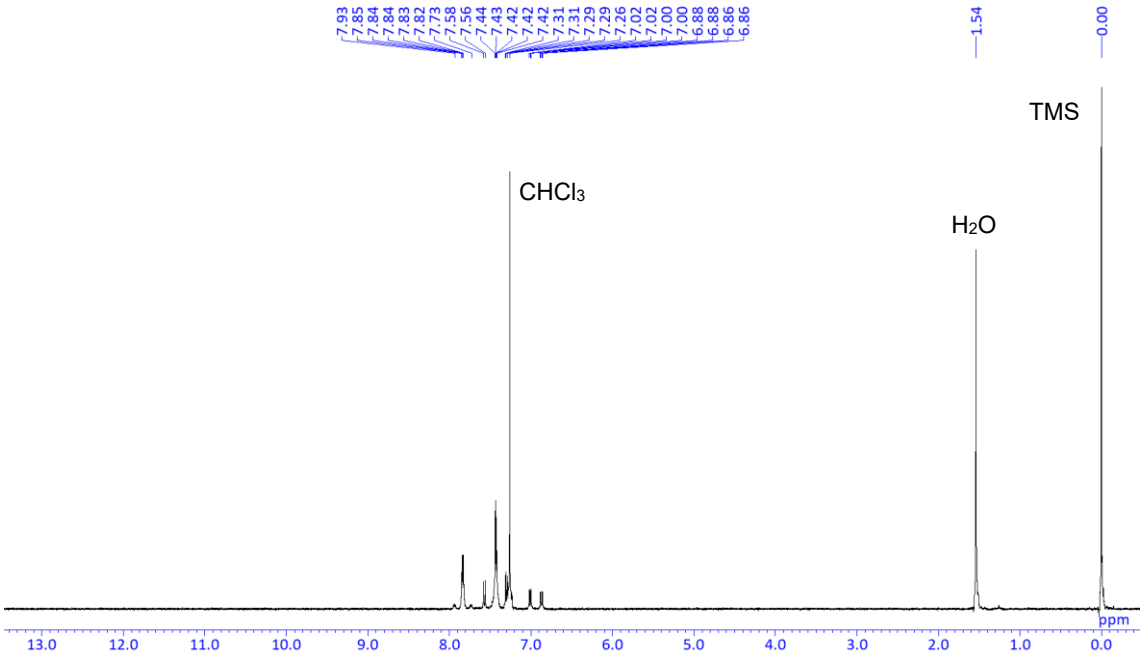

Chart S1. ^{1}H NMR spectrum of **TAzPh** in $CDCl_3$ at 400 MHz.

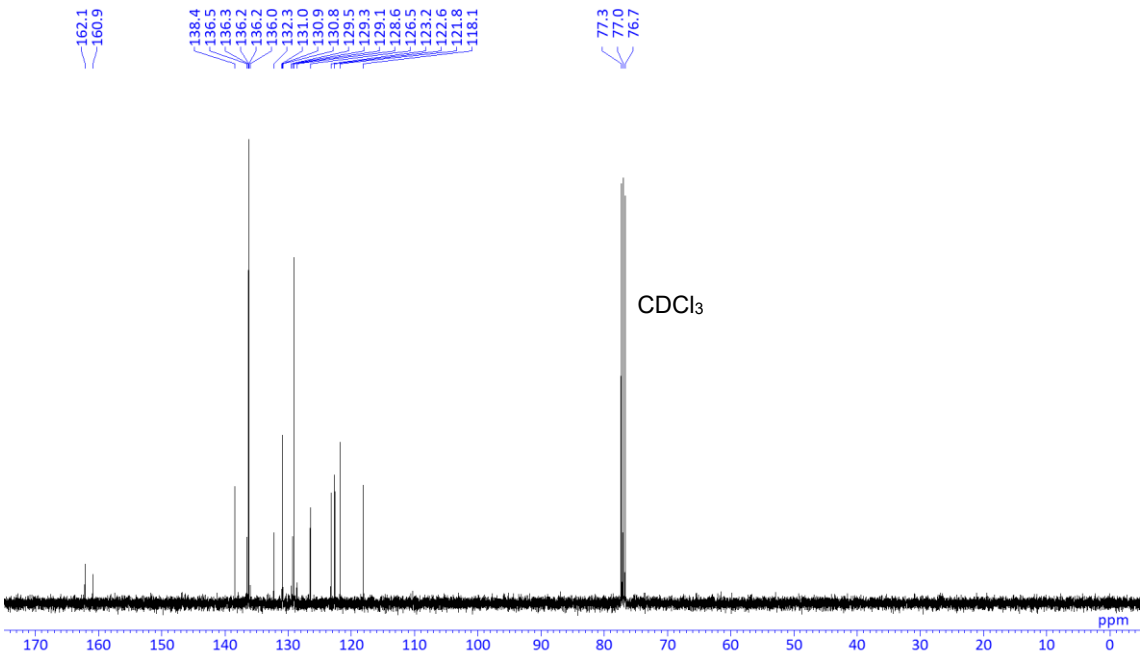

Chart S2. $^{13}C\{^{1}H\}$ NMR spectrum of **TAzPh** in $CDCl_3$ at 100 MHz.

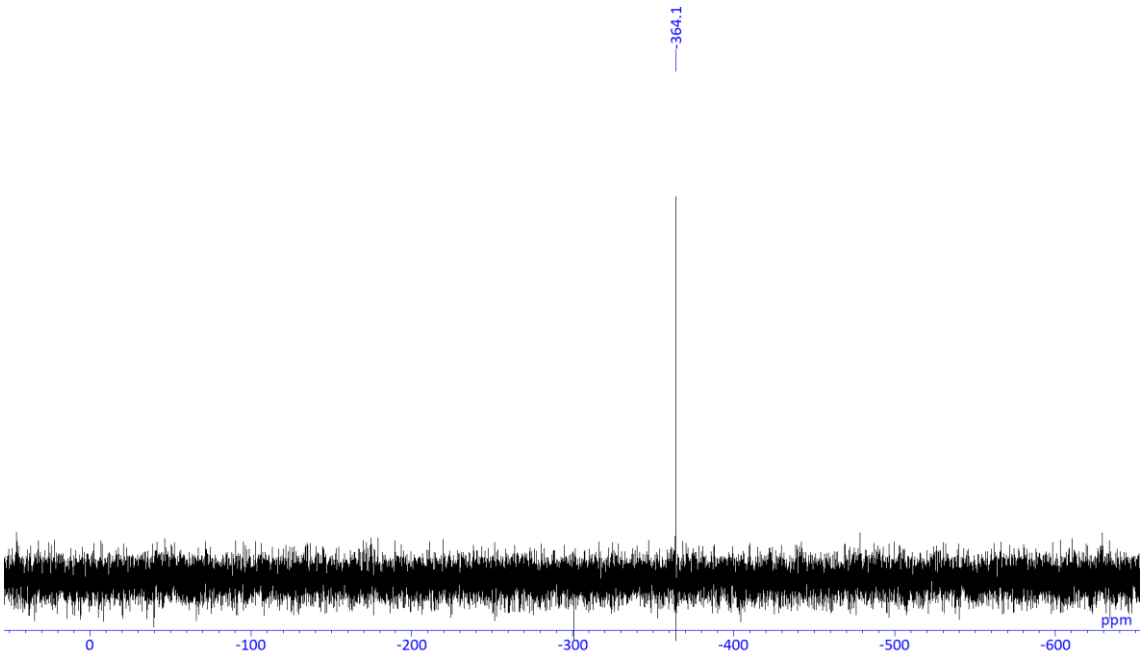

Chart S3. ^{119}Sn NMR spectrum of **TAzPh** in $CDCl_3$ at 149 MHz.

Synthesis of TAzMe

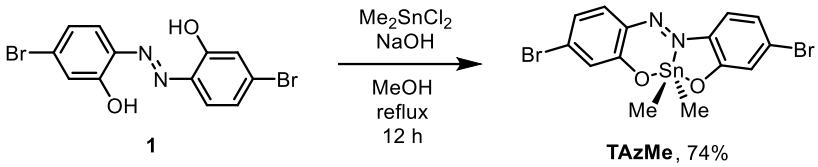

In a 100 mL round bottom flask, **1** (0.559 g, 1.50 mmol, 1 equiv.), dimethyltin(IV)dichloride (0.330 g, 1.50 mmol, 1 equiv.), NaOH (0.120 g, 3.00 mmol, 2 equiv.) and 50 mL of MeOH were added under N_2. Then, the solution was stirred at 80 °C for 12 h. Insoluble materials were filtered, and the solution was concentrated in vacuo. The obtained violet solid was purified by recrystallization with THF and hexane to afford **TAzMe** (0.579 g, 1.12 mmol, 74%) as a black crystal.

^{1}H NMR ($CDCl_3$, 400 MHz) δ 7.58 (d, J = 8.8 Hz, 1H), 7.41 (m, 1H), 7.02 (d, J = 1.7 Hz, 1H), 6.99-6.96 (m, 2H), 6.86 (dd, J = 2.1, 8.6 Hz, 1H), 0.82 (s, $J_{H\text{-}Sn}$ = 38.6 Hz, 6H) ppm. ^{13}C{1H} NMR ($CDCl_3$, 400 MHz) δ 162.0, 160.2, 136.5, 136.2, .135.8, 131.9, 129.2, 126.4, 122.8, 122.4, 121.5, 118.0, 1.8 ppm. ^{119}Sn NMR ($CDCl_3$, 149 MHz) δ −178.3 ppm. HRMS (ESI) calcd. for $C_{14}H_{12}Br_2N_2O_2Sn$ $[M]^-$: 517.8267; found: 517.8266. Elemental analysis calcd. for $C_{14}H_{12}Br_2N_2O_2Sn$: C 32.41 H 2.33 N 5.40 Br 30.80, found: C 32.32 H 2.38 N 5.49 Br 30.61.

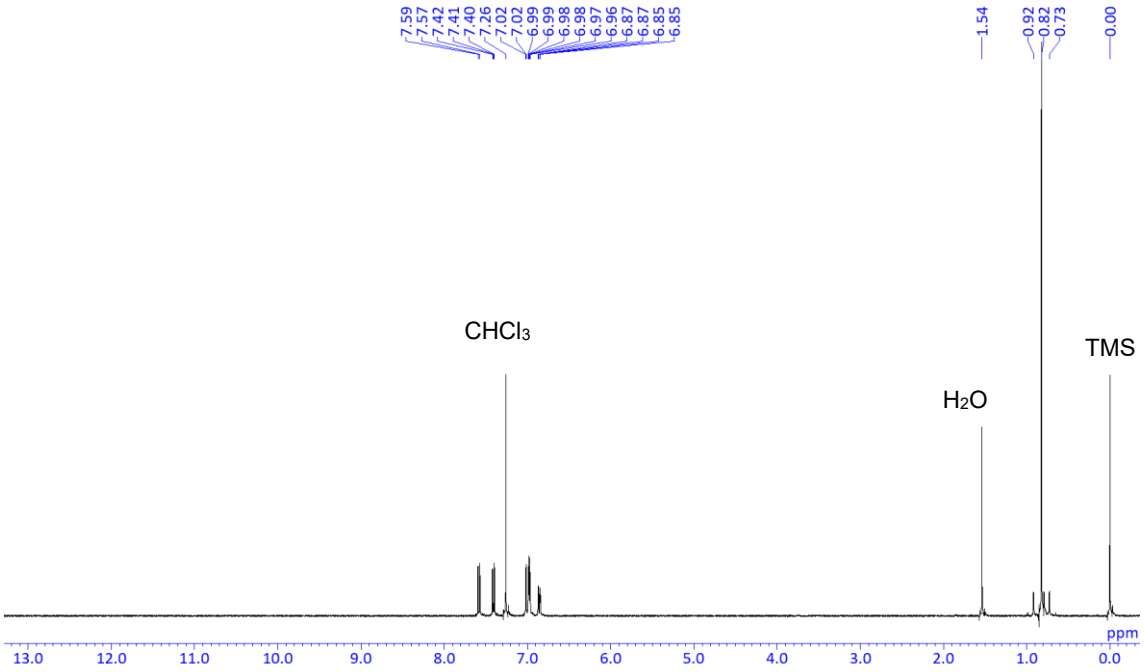

Chart S4. ^{1}H NMR spectrum of **TAzMe** in $CDCl_3$ at 400 MHz.

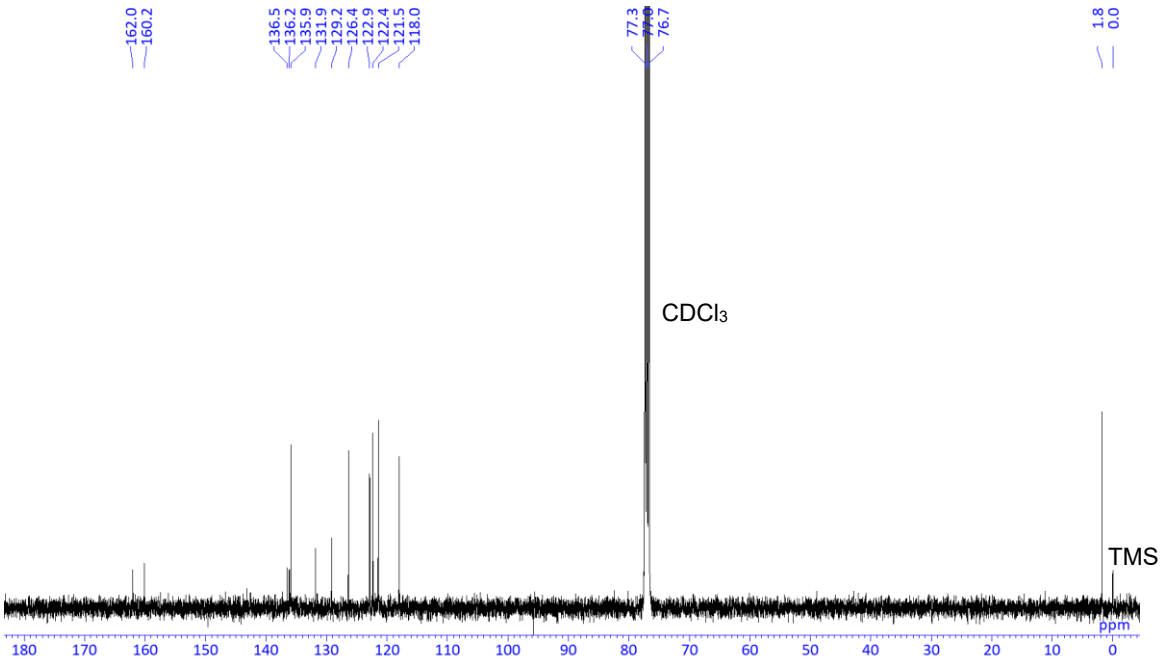

Chart S5. ^{13}C{^{1}H} NMR spectrum of **TAzMe** in $CDCl_3$ at 100 MHz.

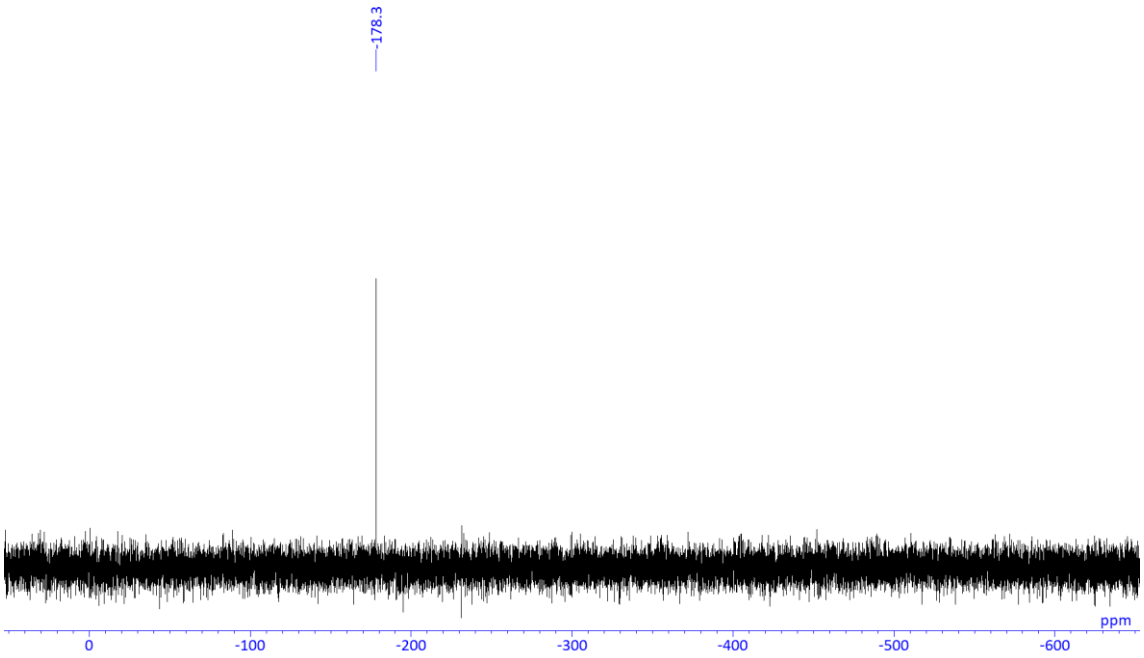

Chart S6. ^{119}Sn NMR spectrum of **TAzMe** in $CDCl_3$ at 149 MHz.

Synthesis of 3

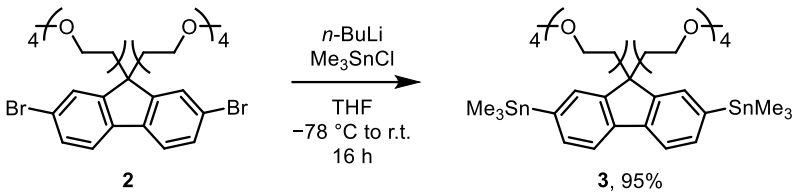

Compound **2** was prepared according to the previous report.[2,3] A solution of *n*-BuLi (1.57 M in hexane, 1.37 mL, 2.14 mmol, 2.2 equiv.) was slowly added to a solution of **2** (0.686 g, 0.974 mmol, 1 equiv.) in THF (40 mL) at −78 °C. After 1 h, trimethyltin chloride (0.485 g, 2.44 mmol, 2.5 equiv.) in THF (10 mL) was added at −78 °C and the mixture was stirred for 16 h at room temperature. Saturated aqueous NH_4Cl was added to the reaction mixture, and the organic layer was extracted with EtOAc. The organic layer was washed with brine and dried over $MgSO_4$. $MgSO_4$ was removed by filtration, and the solvent was removed with a rotary evaporator. The obtained yellow oil **3** (0.805 g, 0.923 mmol, 95%) was used for the next reaction without further purification.

^{1}H NMR ($CDCl_3$, 400 MHz) δ 7.64 (d, J = 7.3 Hz, 2H), 7.49 (s, 2H), 7.44 (d, 2H, J =7.3 Hz), 3.59-3.49 (m, 16H), 3.43-3.39 (m, 4H), 3.35 (s, 6H), 3.24-3.20 (m, 4H), 2.77 (t, J =7.8 Hz, 4H), 2.38 (t, J =7.6 Hz, 4H), 0.33 (m, $J_{H–Sn}$ = 27.4 Hz, 18H) ppm. ^{13}C{^{1}H} NMR ($CDCl_3$, 400 MHz) δ 148.1, 141.6, 140.6, 134.5, 130.1, 119.3, 71.9, 70.5, 70.5, 70.4, 70.4, 69.9, 67.2, 59.0, 51.0, 39.5, −9.3 ($J_{C–Sn}$ = 17.0 Hz) ppm. HRMS (ESI): $[M+Na]^+$ Calcd., 897.2381; Found, 897.2405.

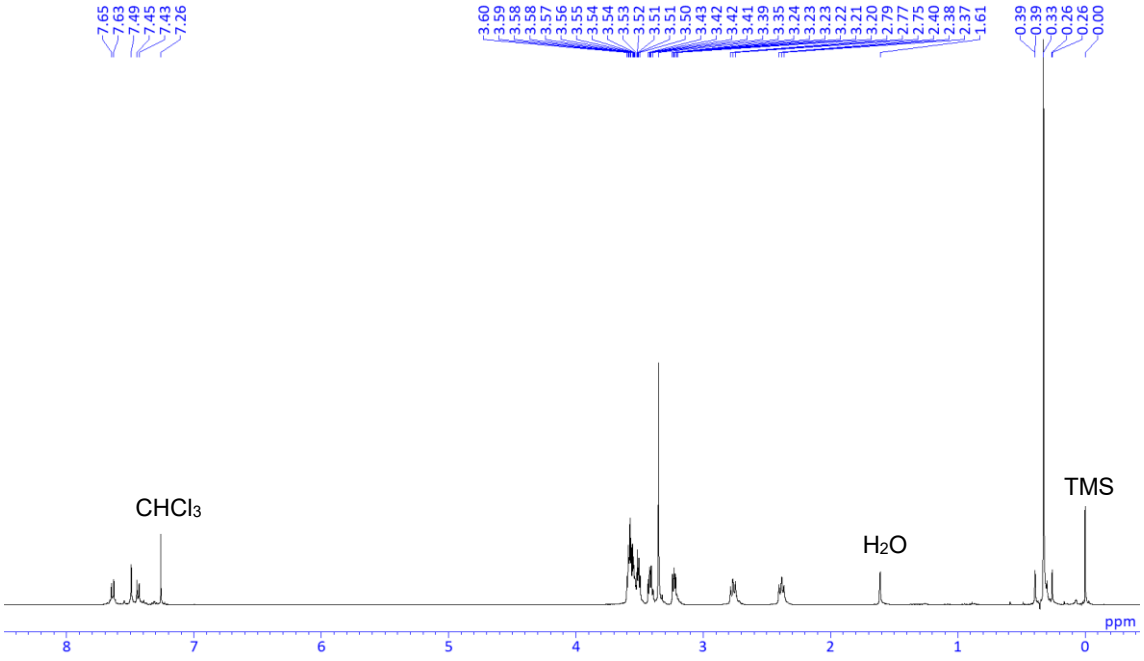

Chart S7. ^{1}H NMR spectrum of **3** in $CDCl_3$ at 400 MHz.

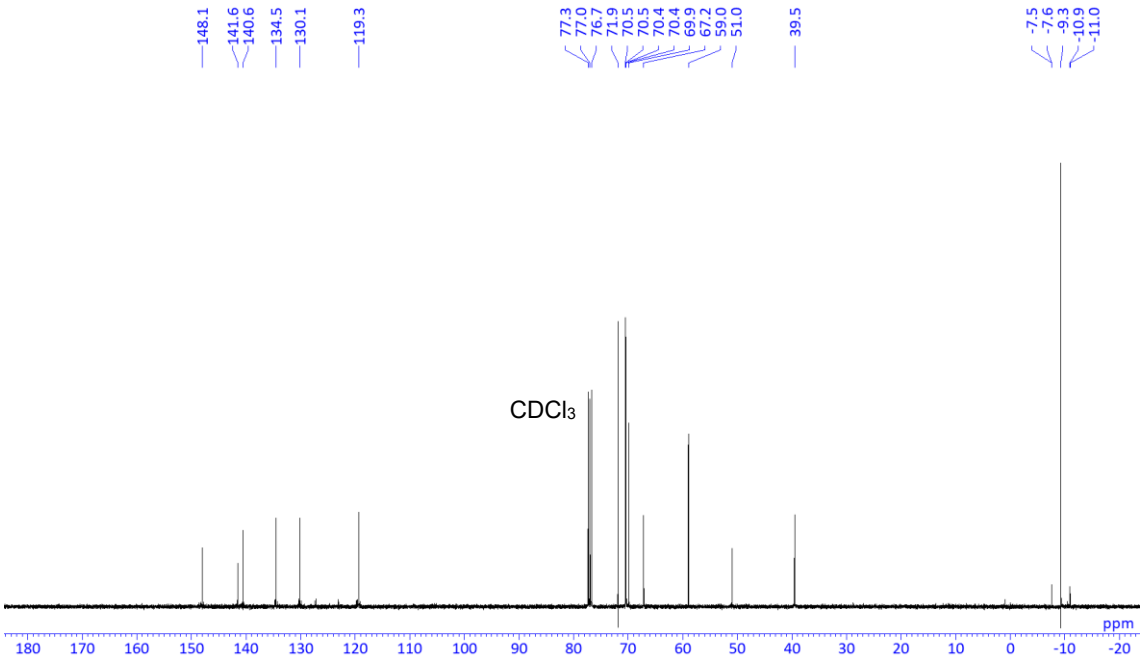

Chart S8. $^{13}C\{^{1}H\}$ NMR spectrum of **3** in $CDCl_3$ at 100 MHz.

Synthesis of P-TAzPh

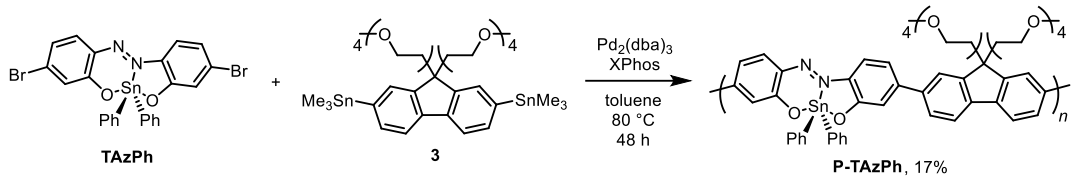

A mixture of **TAzPh** (0.137 g, 0.214 mmol, 1 equiv.), **3** (0.186 g, 0.214 mmol, 1 equiv.), $Pd_2(dba)_3$ (0.0059 g, 0.0064 mmol, 0.03 equiv.), XPhos (0.0061 g, 0.013 mmol, 0.06 equiv.) in toluene (4.0 mL) was stirred at 80 °C for 48 h under N_2 atmosphere. After cooling to room temperature, the solution was poured into a large amount of hexane to collect the polymer by filtration. Additionally, the part of high molecular weight was fractionated by HPLC to afford **P-TAzPh** (0.0381 g, 17%) as a dark blue solid.

M_n = 5,300, M_w = 7,100, M_w/M_n = 1.4. ^{1}H NMR ($CDCl_3$, 400 MHz) δ 8.01 (br), 7.90 (br), 7.79 (br), 7.73 (br), 7.46 (br), 7.15 (br), 3.55 (br), 3.49 (br), 3.42 (br), 3.33 (br), 2.88 (br), 2.53 (br) ppm; ^{13}C{^{1}H} NMR ($CDCl_3$, 100 MHz) δ 136.5, 71.9, 70.5, 70.5, 59.0 ppm. The other ^{13}C{^{1}H} signals were not detected probably because of broadening peaks in a polymer. ^{119}Sn NMR signal was not detected probably because of broadening peaks in a polymer. In place of ^{119}Sn NMR, we confirmed the preservation of tin atom after polymerization by detection of repeating units from a MALDI-TOF MS measurement (negative, matrix: *trans*-2-[3-(4-*tert*-Butylphenyl)-2-methyl-2-propenylidene]malononitrile (DCTB)).

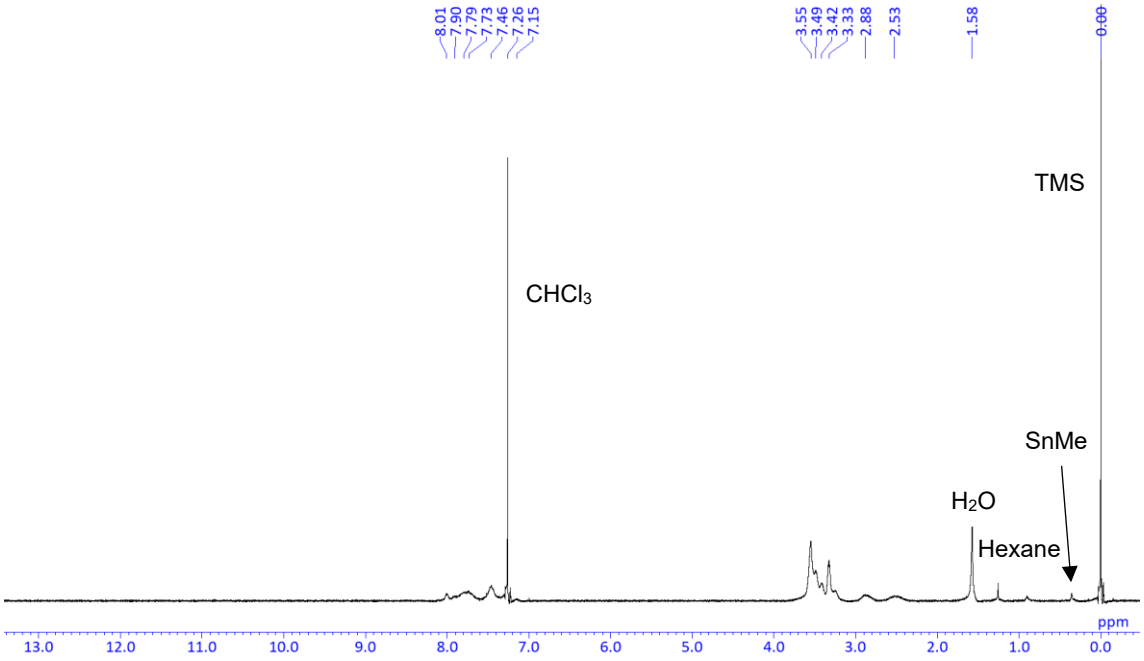

Chart S9. ^{1}H NMR spectrum of **P-TAzPh** in $CDCl_3$ at 400 MHz.

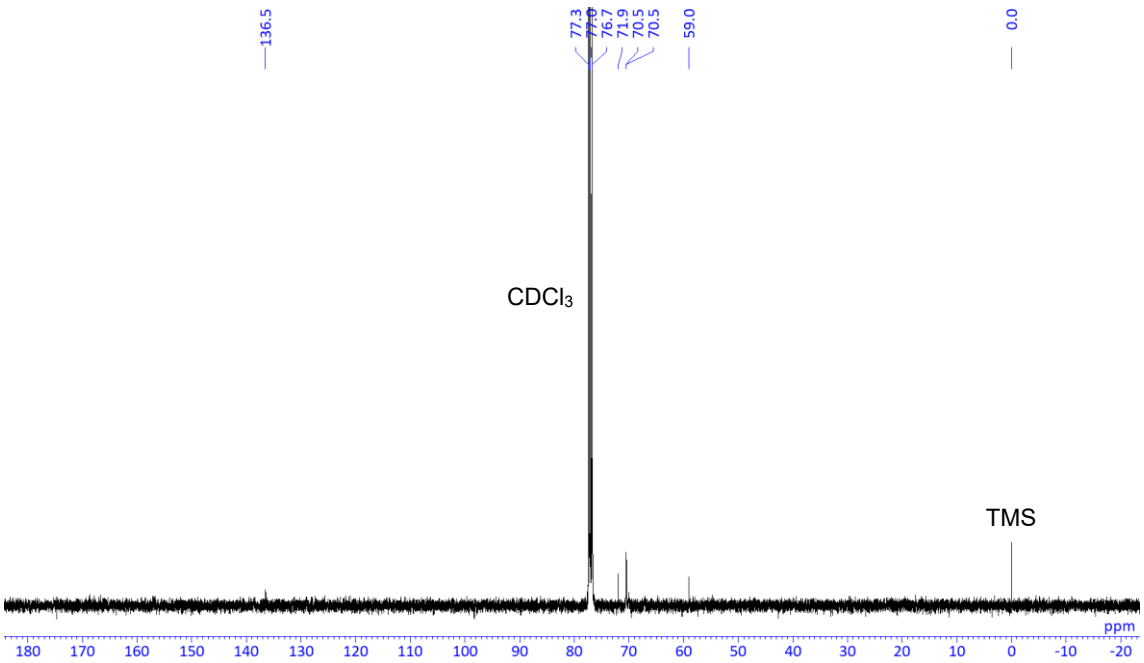

Chart S10. $^{13}C\{^{1}H\}$ NMR spectrum of **P-TAzPh** in $CDCl_3$ at 100 MHz.

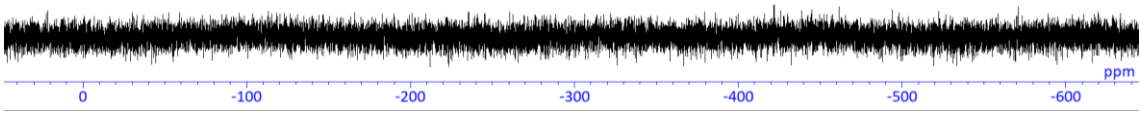

Chart S11. ^{119}Sn NMR spectrum of **P-TAzPh** in $CDCl_3$ at 149 MHz.

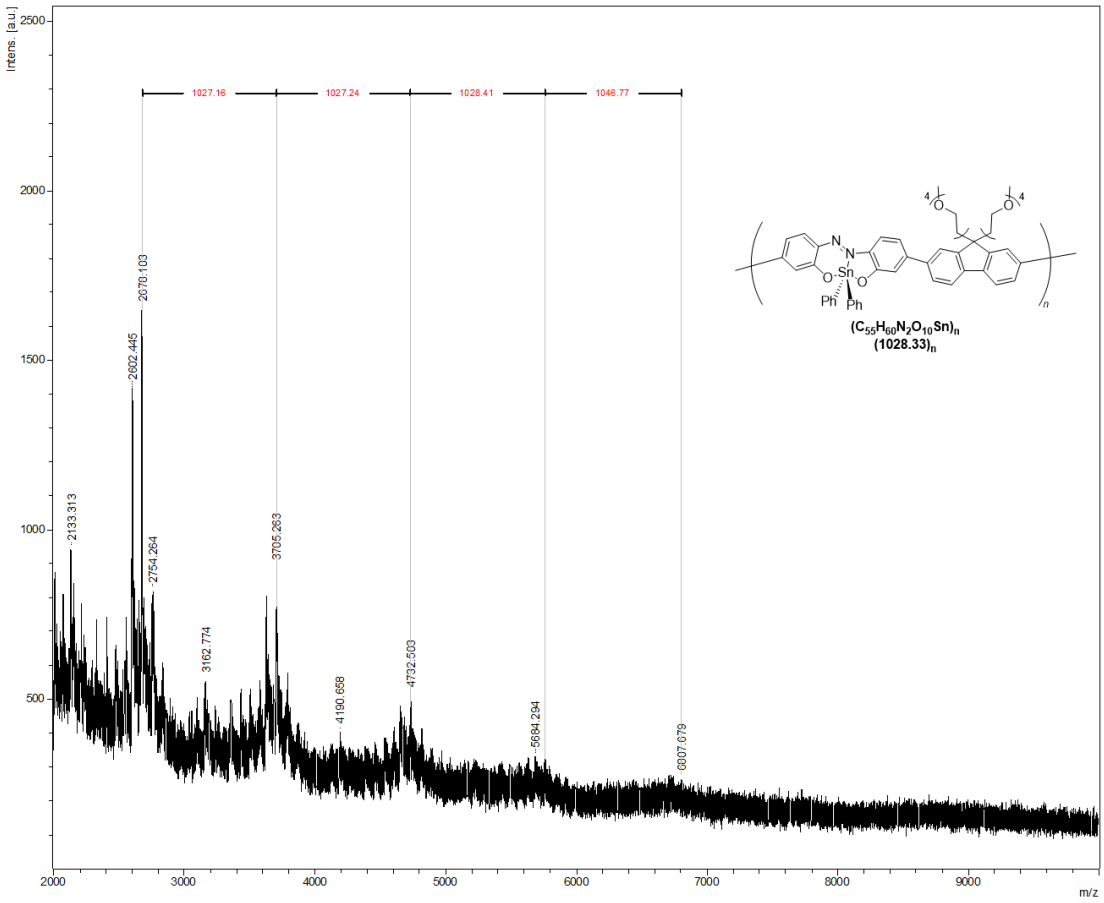

Chart S12. MADLI-TOF MS spectrum of **P-TAzPh**.

Synthesis of P-TAzMe

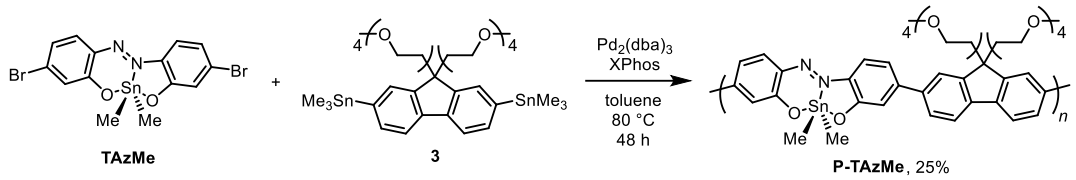

A mixture of **TAzMe** (0.107 g, 0.205 mmol, 1 equiv.), **3** (0.179 g, 0.205 mmol, 1 equiv.), $Pd_2(dba)_3$ (0.0056 g, 0.0062 mmol, 0.03 equiv.), XPhos (0.0059 g, 0.012 mmol, 0.06 equiv.) in toluene (4.0 mL) was stirred at 80 °C for 48 h under N_2 atmosphere. After cooling to room temperature, the solution was poured into a large amount of hexane to collect the polymer by filtration. Additionally, the part of high molecular weight was fractionated by HPLC to afford **P-TAzMe** (0.0463 g, 25%) as a dark blue solid.

M_n = 6,200, M_w = 8,200, M_w/M_n = 1.3. ^{1}H NMR ($CDCl_3$, 400 MHz) δ 7.92 (br), 7.79 (br), 7.76 (br), 7.72 (br), 7.19 (br), 7.15 (br), 3.57-3.50 (m), 3.40 (br), 3.34 (t), 3.22 (br), 2.85 (br), 2.48 (br), 0.91-0.84 (m) ppm; $^{13}C\{^1H\}$ NMR ($CDCl_3$, 100 MHz) δ 126.8, 117.4, 71.9, 70.5, 70.5, 70.5, 70.4, 70.0 (br), 67.1 (br), 59.0, 1.5 ppm. The other $^{13}C\{^1H\}$ signals were not detected probably because of broadening peaks in a polymer. ^{119}Sn NMR ($CDCl_3$, 149 MHz) δ −179.9 (br). We also confirmed the preservation of tin atom after polymerization by detection of repeating units from a MALDI-TOF MS measurement (negative, matrix: *trans*-2-[3-(4-*tert*-Butylphenyl)-2-methyl- 2-propenylidene]malononitrile (DCTB)).

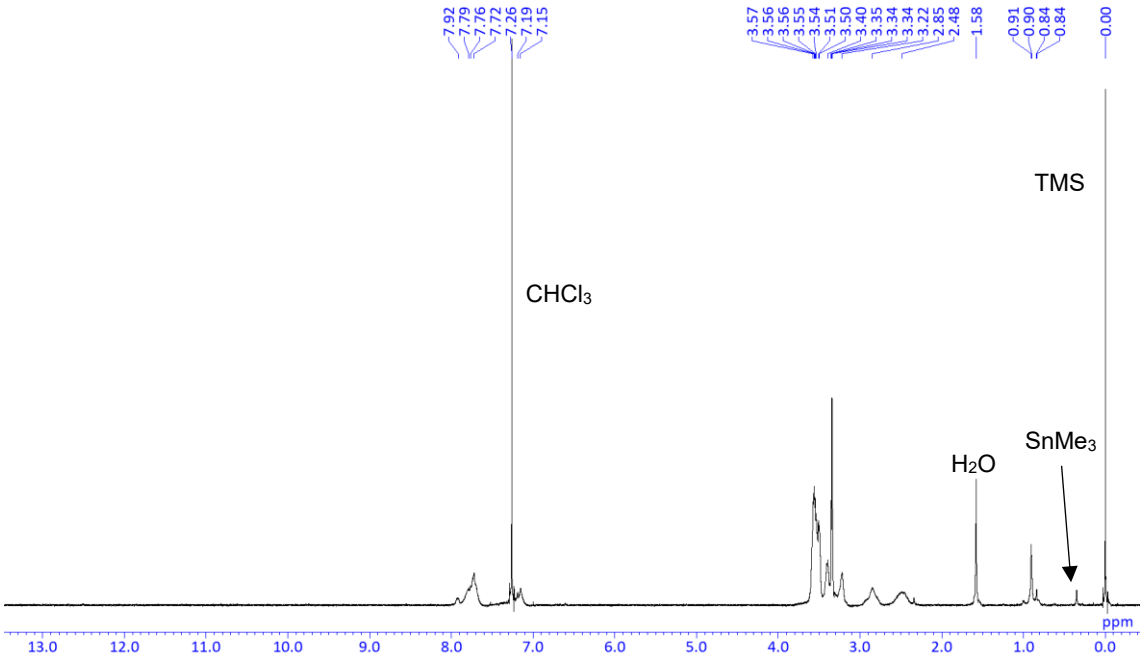

Chart S13. ^{1}H NMR spectrum of **P-TAzMe** in $CDCl_3$ at 400 MHz.

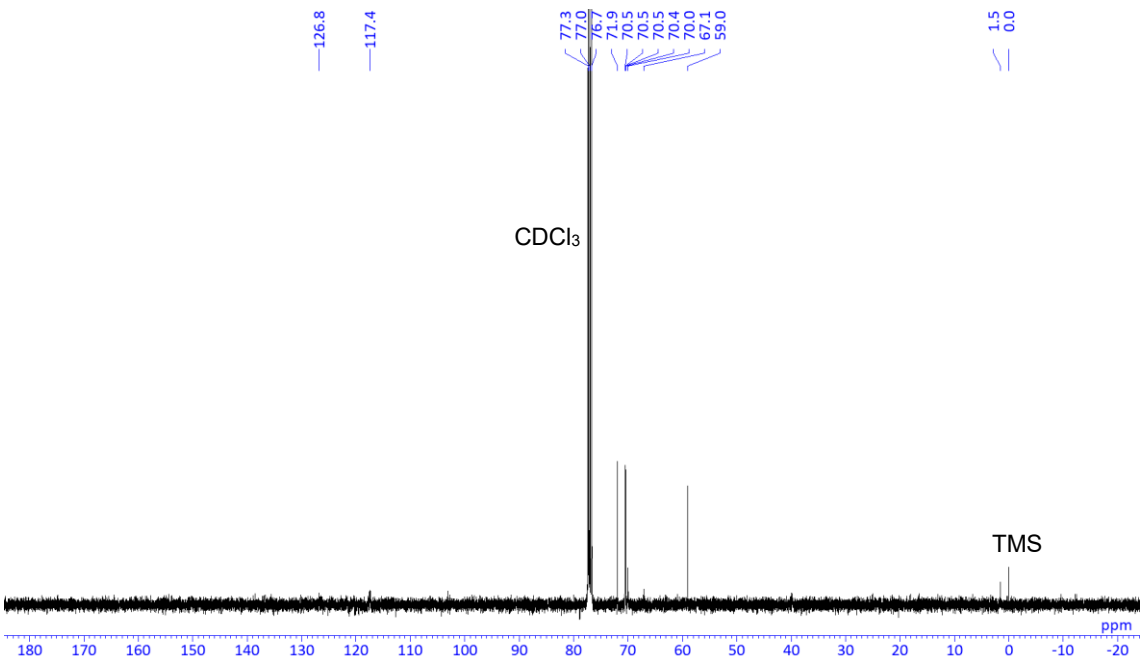

Chart S14. $^{13}C\{^{1}H\}$ NMR spectrum of **P-TAzMe** in $CDCl_3$ at 100 MHz.

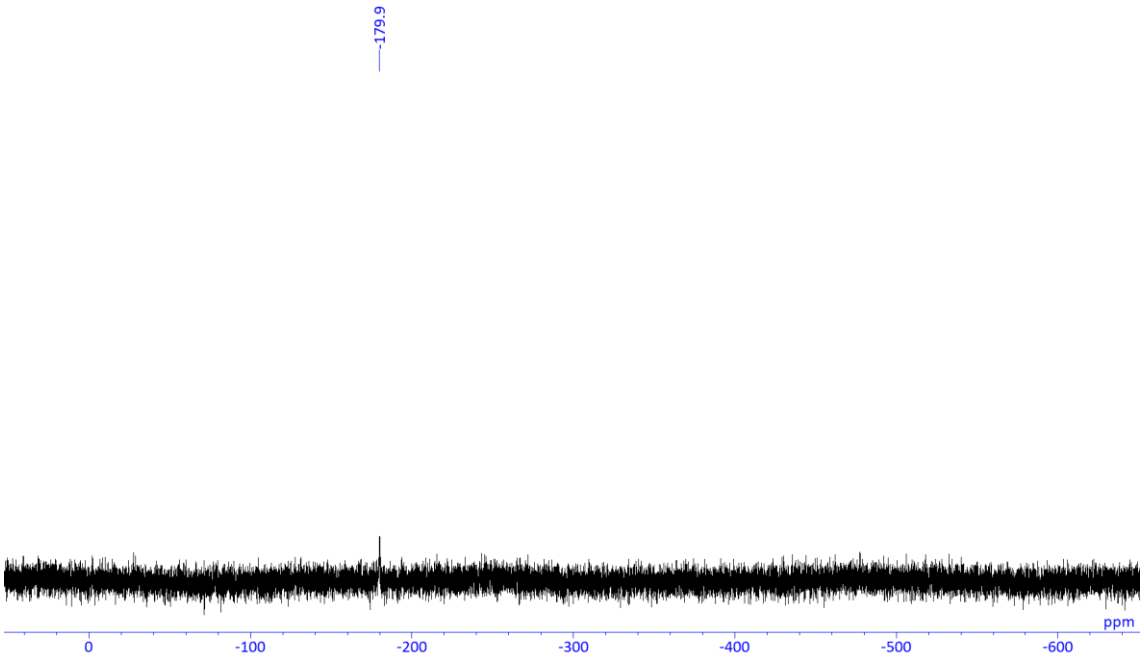

Chart S15. ^{119}Sn NMR spectrum of **P-TAzMe** in $CDCl_3$ at 149 MHz.

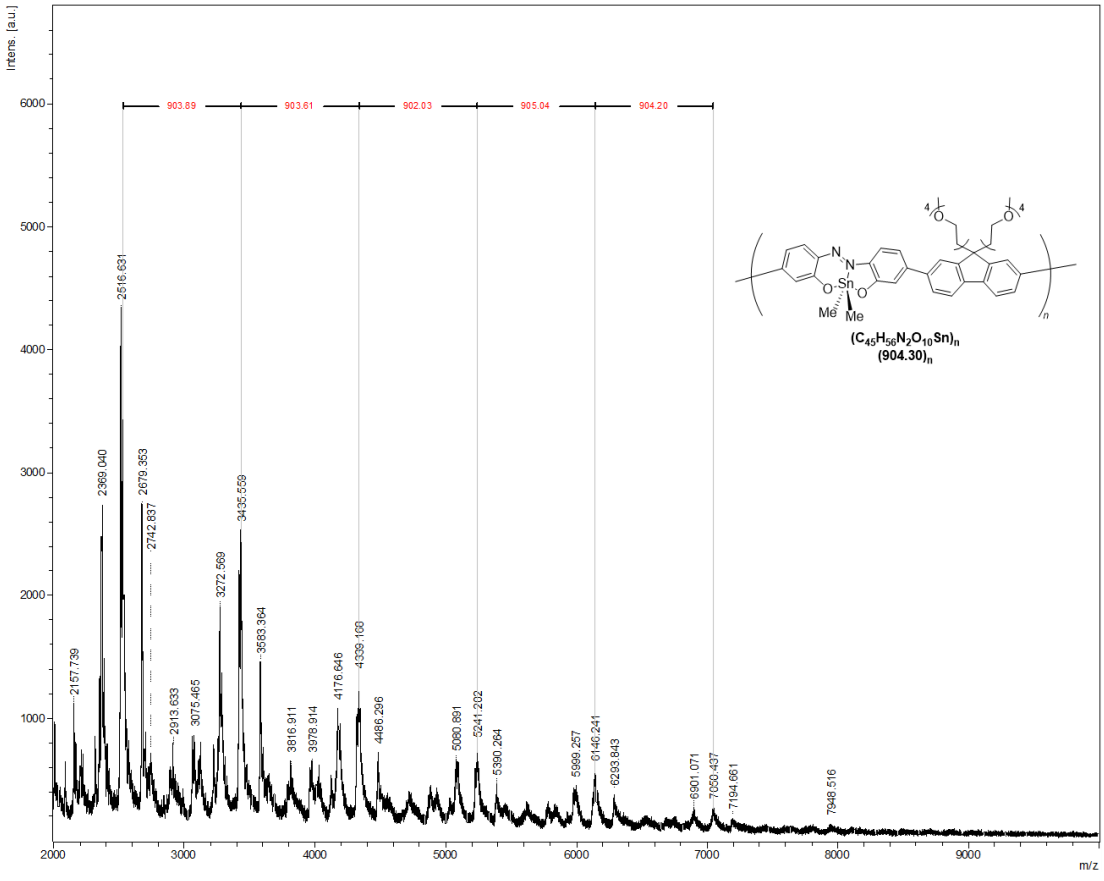

Chart S16. MADLI-TOF MS spectrum of **P-TAzMe**.

Solvent effect

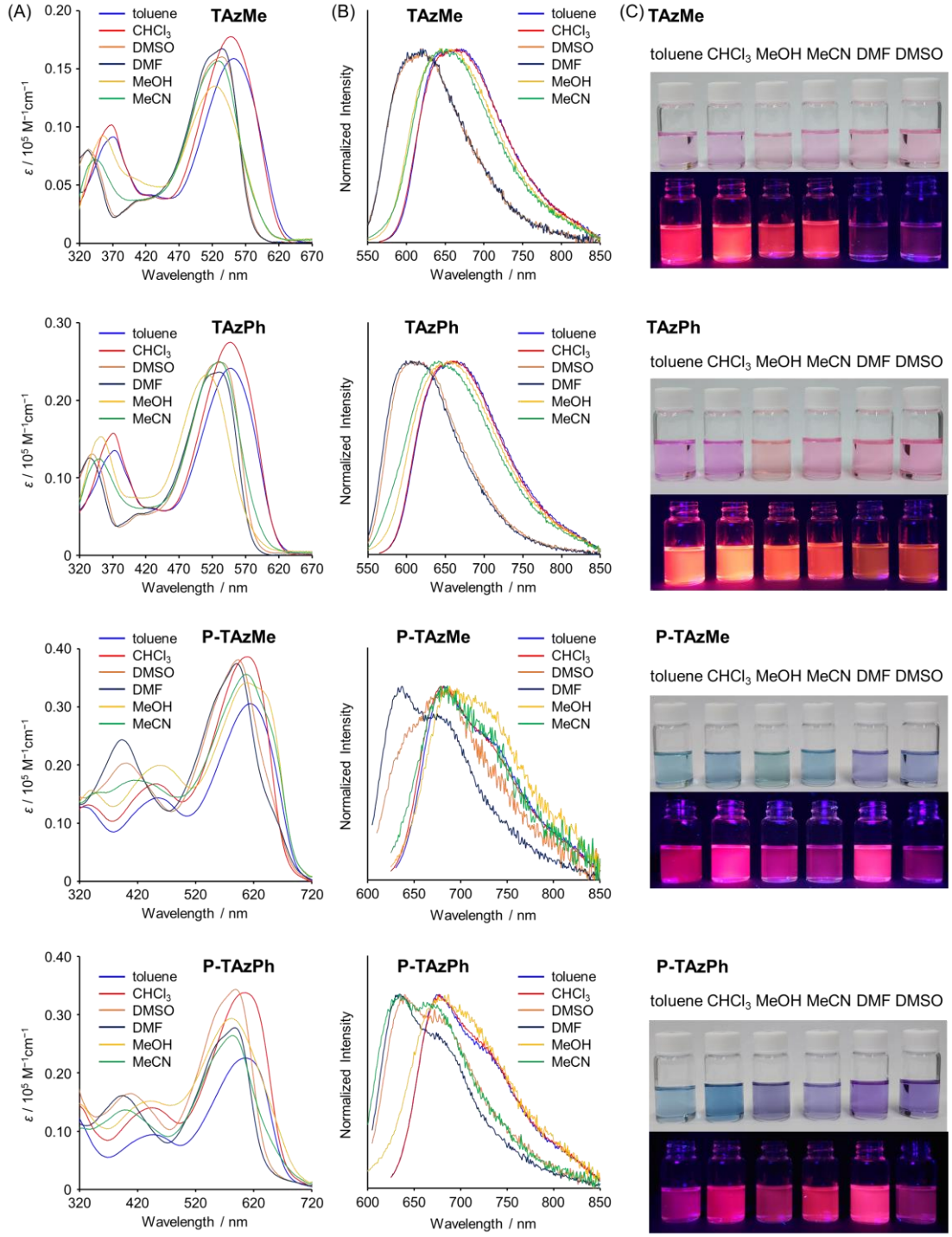

Figure S1. (A) UV–vis absorption and (B) PL spectra and (C) photographs under room light (upper) and irradiated by 365 nm (below) of **TAzMe**, **TAzPh**, **P-TAzMe** and **P-TAzPh** (1.0×10^{-5} M for monomers and 1.0×10^{-5} M per repeating unit for polymers) in toluene and $CHCl_3$ and toluene/solvents(DMSO, DMF, MeOH, MeCN) = 99/1 v/v.

Titration

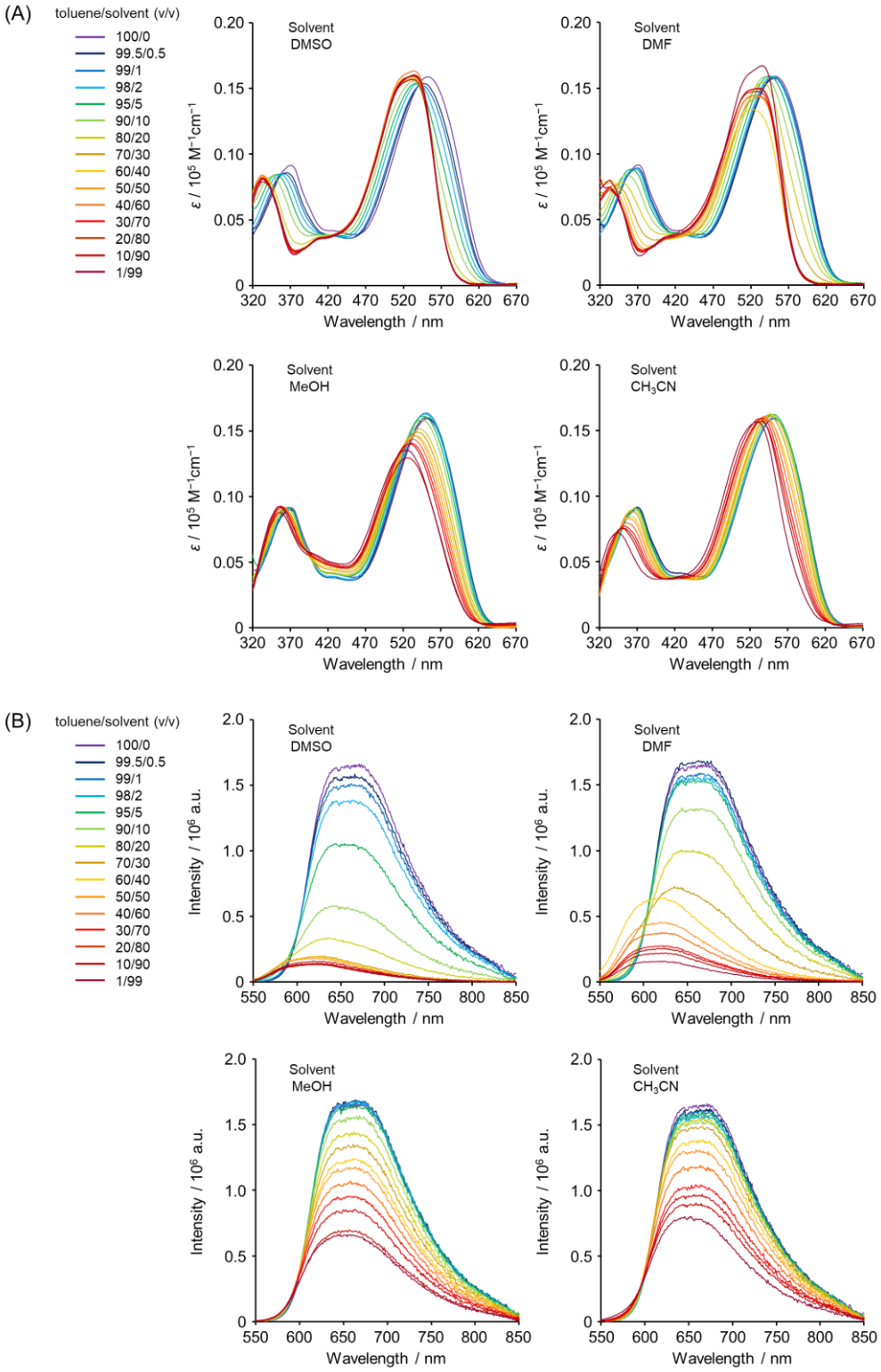

Figure S2. Titration spectra of (A) UV–vis absorption and (B) PL of **TAzMe** in mixed solvents (1.0×10^{-5} M).

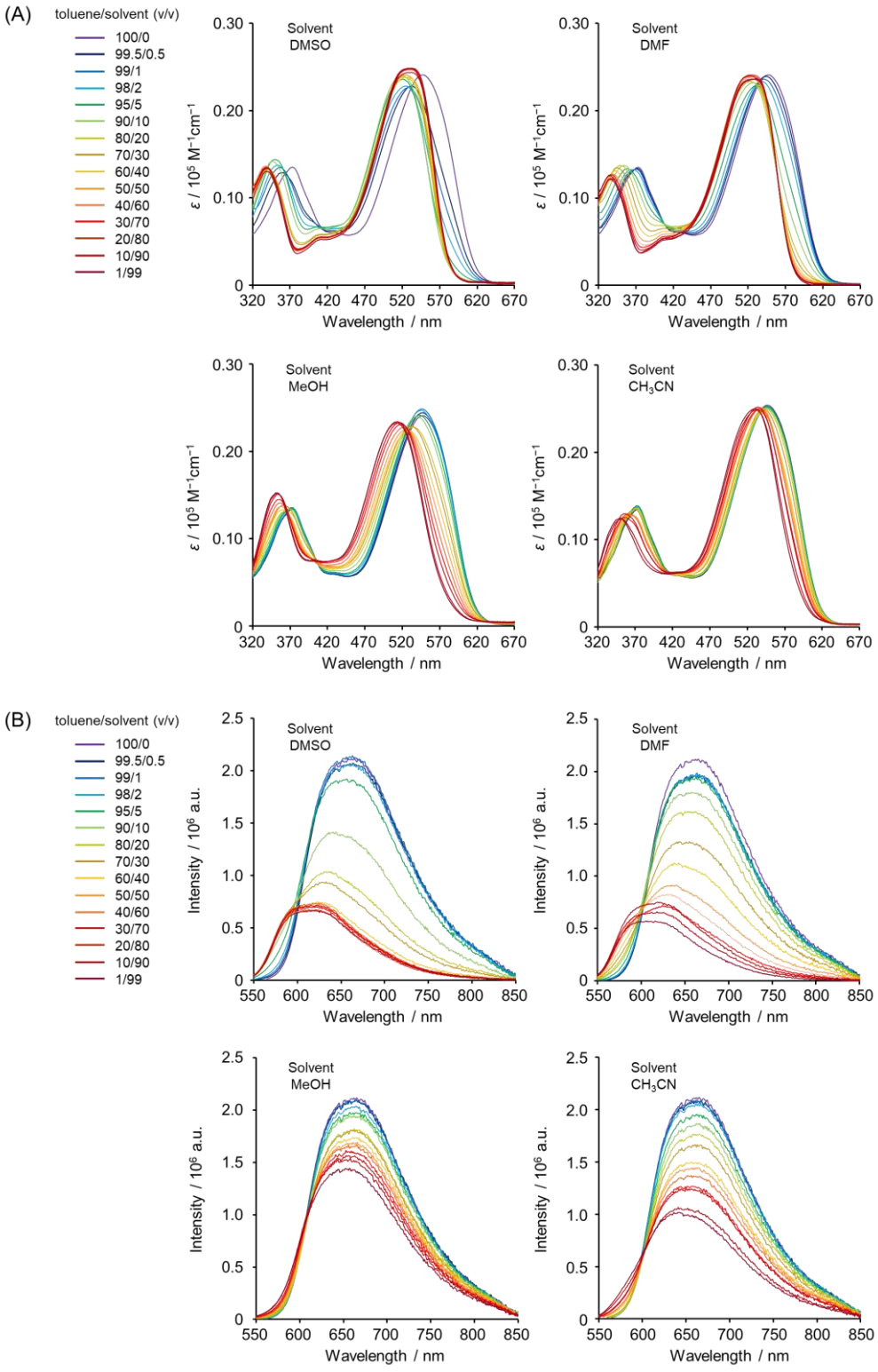

Figure S3. Titration spectra of (A) UV–vis absorption and (B) PL of **TAzPh** in mixed solvents (1.0×10^{-5} M).

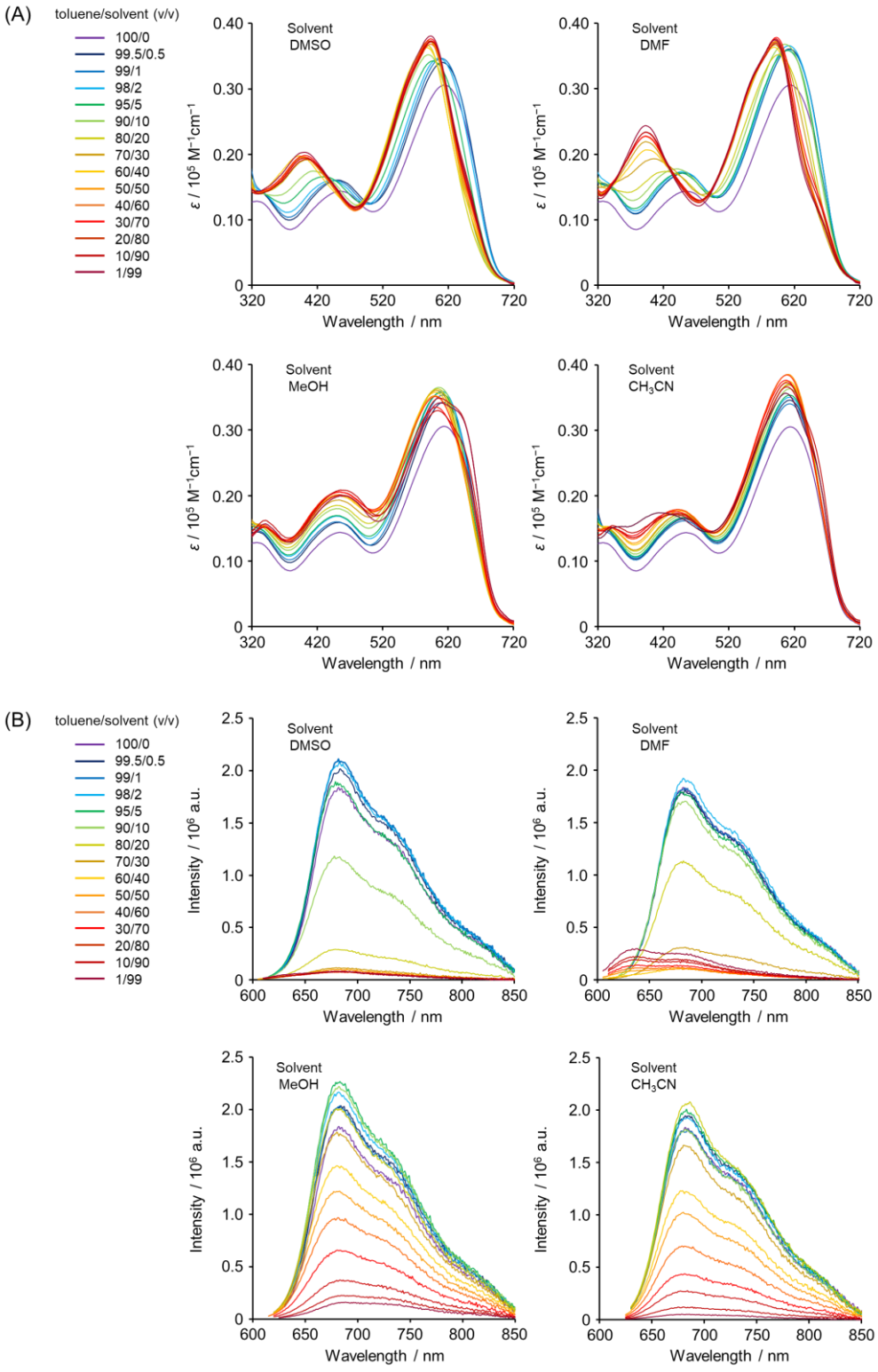

Figure S4. Titration spectra of (A) UV–vis absorption and (B) PL of **P-TAzMe** in mixed solvents (1.0×10^{-5} M per repeating unit).

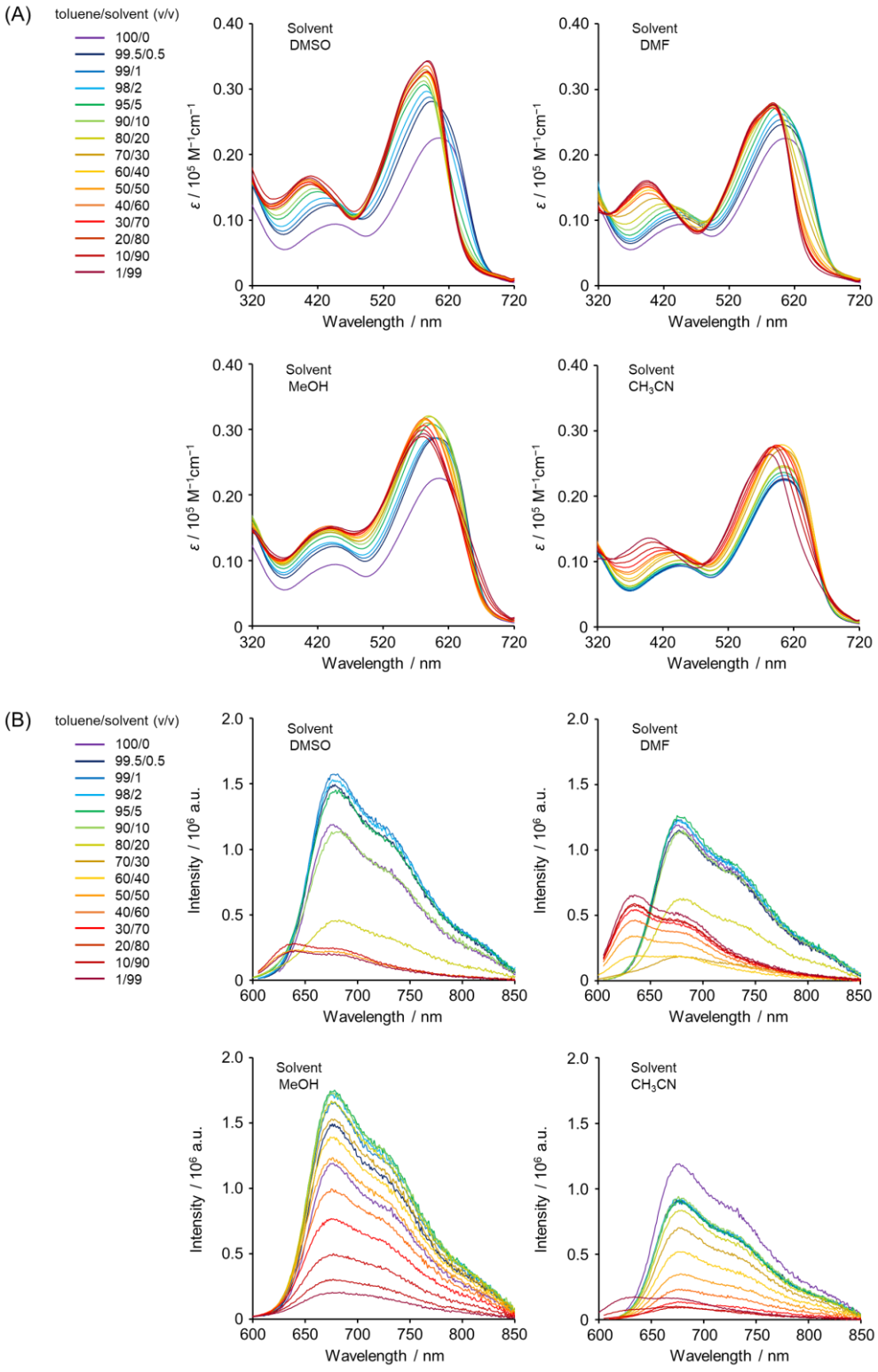

Figure S5. Titration spectra of (A) UV–vis absorption and (B) PL of **P-TAzPh** in mixed solvents (1.0×10^{-5} M per repeating unit).

Summary of absolute PL quantum yields of TAz compounds

Table S1. Absolute PL quantum yields (%) of **TAzMe**[a]

Solvent vol%	0	0.5	1	2	5	10	20	30	40	50	60	70	80	90	99
toluene	18.0[b]	–	–	–	–	–	–	–	–	–	–	–	–	–	–
$CHCl_3$	16.5[b]	–	–	–	–	–	–	–	–	–	–	–	–	–	–
DMSO	–	16.3	15.6	13.9	9.4	4.7	2.0	1.5	1.5	1.6	1.2	1.2	1.2	1.4	1.3
DMF	–	16.7	16.5	16.4	15.1	12.4	8.6	4.4	4.1	3.2	2.8	1.9	1.7	1.7	1.3
MeOH	–	17.4	17.5	17.0	16.1	15.2	13.9	12.5	11.4	9.8	8.7	7.5	6.5	5.6	4.8
MeCN	–	17.2	17.0	16.7	16.5	15.8	14.8	13.7	12.4	11.6	9.1	6.9	5.8	4.7	4.0

[a] Measured in mixed solutions (1.0×10^{-5} M, toluene/solvent) excited at absorption maxima.

[b] In pure toluene or $CHCl_3$.

Table S2. Absolute PL quantum yields (%) of **TAzPh**[a]

Solvent vol%	0	0.5	1	2	5	10	20	30	40	50	60	70	80	90	99
toluene	15.6[a]	–	–	–	–	–	–	–	–	–	–	–	–	–	–
$CHCl_3$	15.7[a]	–	–	–	–	–	–	–	–	–	–	–	–	–	–
DMSO	–	15.5	15.3	14.5	12.3	7.8	4.6	3.9	3.8	4.0	3.7	3.7	3.8	3.5	3.7
DMF	–	15.4	15.5	15.1	14.1	12.1	10.0	7.2	5.1	3.7	3.6	3.5	3.7	3.7	4.1
MeOH	–	15.5	15.1	14.8	14.0	13.4	12.2	11.7	10.7	9.8	8.9	8.3	7.4	6.9	6.7
MeCN	–	15.5	15.0	14.8	14.4	13.6	12.3	11.1	9.7	8.7	8.0	7.0	6.4	5.1	4.1

[a] Measured in mixed solutions (1.0×10^{-5} M, toluene/solvent) excited at absorption maxima.

[b] In pure toluene or $CHCl_3$.

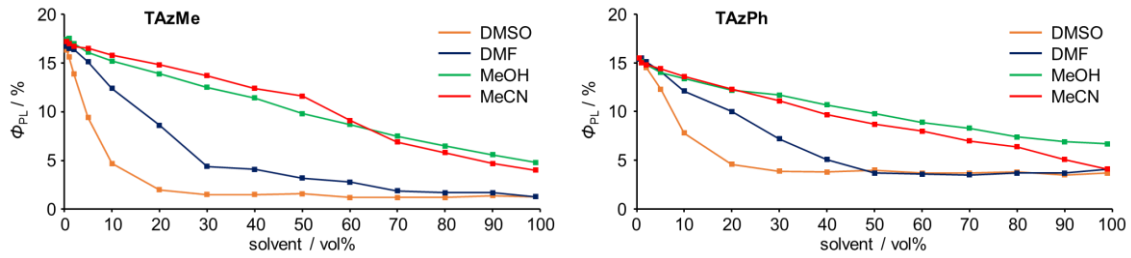

Figure S6. Plots of absolute PL quantum yields (%) versus solvents (vol%) in toluene (1.0×10^{-5} M per repeating unit) from Tables S1 and S2.

Table S3. Absolute PL quantum yields (%) of **P-TAzMe**[a]

Solvent vol%	0	0.5	1	2	5	10	20	30	40	50	60	70	80	90	99
toluene	24.4[b]	–	–	–	–	–	–	–	–	–	–	–	–	–	–
$CHCl_3$	31.2[b]	–	–	–	–	–	–	–	–	–	–	–	–	–	–
DMSO	–	27.0	26.8	26.5	22.0	10.0	2.4	1.2	1.1	0.9	1.1	1.1	1.0	0.9	1.0
DMF	–	27.0	26.5	26.3	24.5	22.5	12.7	2.3	1.2	1.3	1.8	2.0	2.4	2.5	2.6
MeOH	–	25.7	26.1	26.6	27.3	25.9	23.1	19.7	16.6	13.1	10.8	7.5	4.5	2.9	2.0
MeCN	–	28.2	26.9	29.0	27.7	25.2	25.1	20.8	16.0	12.1	8.8	5.0	2.5	1.1	0.7

[a] Measured in mixed solutions (1.0×10^{-5} M per repeating unit, toluene/solvent) excited at absorption maxima.

[b] In pure toluene or $CHCl_3$.

Table S4. Absolute PL quantum yields (%) of **P-TAzPh**[a]

Solvent vol%	0	0.5	1	2	5	10	20	30	40	50	60	70	80	90	99
toluene	19.2[a]	–	–	–	–	–	–	–	–	–	–	–	–	–	–
$CHCl_3$	16.7[a]	–	–	–	–	–	–	–	–	–	–	–	–	–	–
DMSO	–	18.8	17.5	16.6	14.3	10.2	3.6	2.0	2.5	2.4	2.6	2.4	2.9	2.1	2.2
DMF	–	17.4	16.8	15.9	14.9	13.1	6.0	1.8	2.3	3.7	4.8	5.0	5.0	4.9	5.1
MeOH	–	18.3	19.0	19.2	18.0	16.5	15.1	13.1	11.8	10.1	8.0	6.2	4.2	2.5	1.6
MeCN	–	18.6	18.2	18.2	17.8	15.8	13.5	10.2	7.1	4.1	2.5	1.5	1.4	1.3	1.2

[a] Measured in mixed solutions (1.0×10^{-5} M per repeating unit, toluene/solvent) excited at absorption maxima.

[b] In pure toluene or $CHCl_3$.

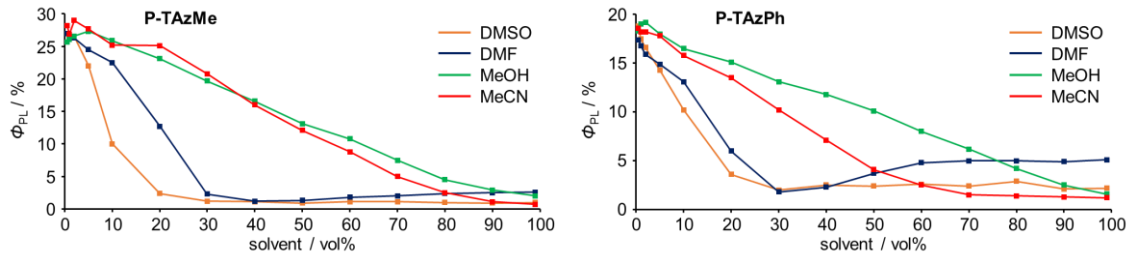

Figure S7. Plots of absolute PL quantum yields (%) versus solvents (vol%) in toluene (1.0×10^{-5} M per repeating unit) from Tables S3 and S4.

Determination of binding constant

Determination of binding constants for the TAz complexes was carried out by means of an absorption titration technique in toluene at room temperature (25 °C) (Figure S8) according to our previous research.[5] We assumed equilibrium 1:1 binding of a TAz complex and a solvent (Scheme S1). The concentration of a TAz complex, $[H]_0$ was kept constant and the concentration of guest (DMSO or DMF), $[G]$, was varied in non-coordinating solvent, toluene. The mixed solutions of a TAz complex and guest from toluene/guest = 100/0 to 1/99 v/v were prepared, and UV–vis absorption spectra were recorded. The host-guest complexation immediately reach equilibrium after preparation of the mixed solutions. The binding constants were determined by a non-linear curve fitting analysis of hypsochromic shifts and reduction of absorption spectra by increasing guest concentration from toluene/solvent = 100/0 to 9/1 v/v solutions because the raising solvent polarity affected the shape of absorption spectra over toluene/solvent = 9/1 v/v solution components. The y-axis is ΔA and the x-axis is $[G]$. The binding constants $K_{a,guest}$ were calculated from eq(1) using non-linear curve fitting (A: absorbance, b: optical path length, ε: molar extinction coefficient, $\Delta\varepsilon = \varepsilon(100/0) - \varepsilon(1/99)$). A(x/y) or ε(x/y) means a value of an absorbance or a molar extinction coefficient of a sample in toluene/solvent = x/y v/v, respectively.

$$\Delta A = (b\Delta\varepsilon/2K_{guest})[1 + K_{a,guest}[G] + K_{guest}[H_0] - \{(1 + K_{guest}[H_0] + K_{guest}[G])^2 - 4K_{guest}^2[G][H_0]\}^{1/2}] \quad (1)$$

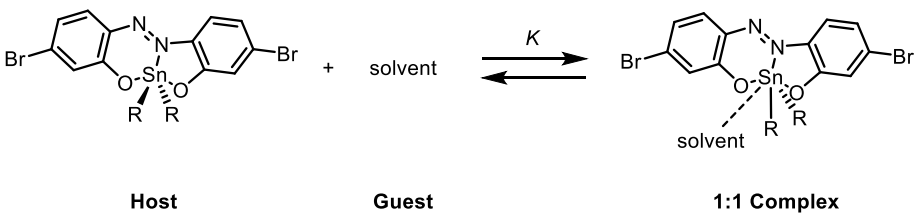

Scheme S1. Equilibrium reaction between host TAz complexes (R = Me, Ph) and guest solvents (DMSO, DMF).

TAzMe in DMSO

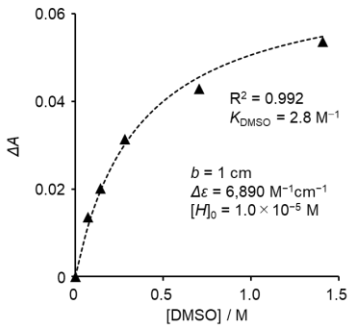

toluene/DMSO v/v	[DMSO] / M	ΔA^a
100/0	0	0
99.5/0.5	0.070	0.0136
99/1	0.14	0.0201
98/2	0.28	0.0314
95/5	0.70	0.0429
9/1	1.4	0.0536

[a] $\Delta A = A(100/0) - A$, at 600 nm

TAzMe in DMF

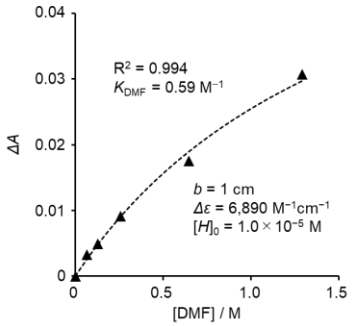

toluene/DMF v/v	[DMF] / M	ΔA^a
100/0	0	0
99.5/0.5	0.065	0.0033
99/1	0.13	0.0049
98/2	0.26	0.0091
95/5	0.65	0.0175
9/1	1.3	0.0307

[a] $\Delta A = A(100/0) - A$, at 600 nm

TAzPh in DMSO

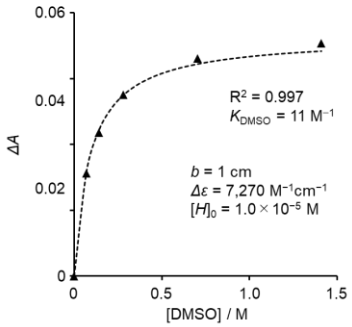

toluene/DMSO v/v	[DMSO] / M	ΔA^a
100/0	0	0
99.5/0.5	0.070	0.0312
99/1	0.14	0.0435
98/2	0.28	0.0551
95/5	0.70	0.0662
9/1	1.4	0.0707

[a] $\Delta A = A(100/0) - A$, at 600 nm

TAzPh in DMF

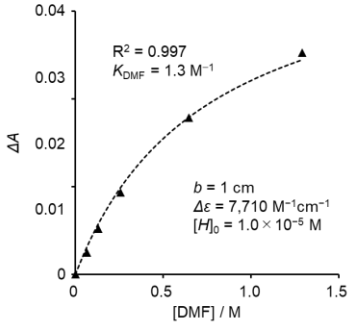

toluene/DMF v/v	[DMF] / M	ΔA^a
100/0	0	0
99.5/0.5	0.065	0.005
99/1	0.13	0.0104
98/2	0.26	0.0187
95/5	0.65	0.0358
9/1	1.3	0.0506

[a] $\Delta A = A(100/0) - A$, at 600 nm

Figure S8. Absorption titration and non-linear curve fitting graph and parameters of **TAzMe** and **TAzPh** with DMSO and DMF in toluene at room temperature.

Vapochromism of film

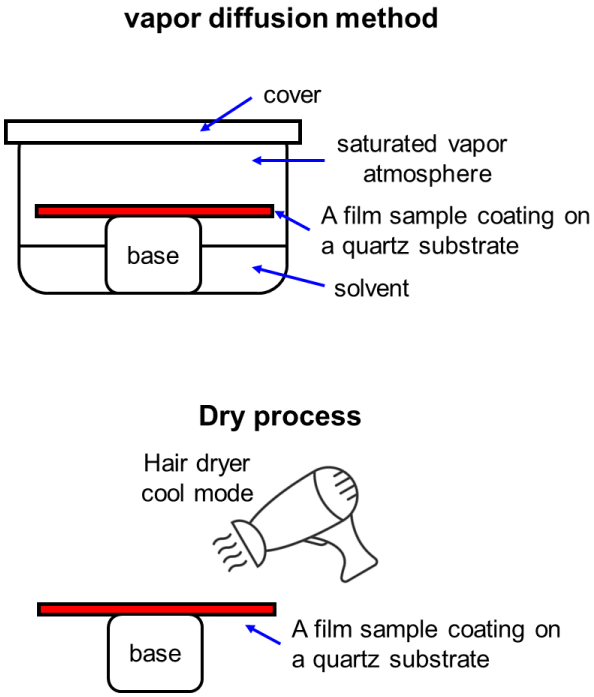

Figure S9. Schematic illustration of vapor diffusion method (30 min) and dry process (30 min) to investigate vapochromism in film.

UV−vis absorption spectra in film

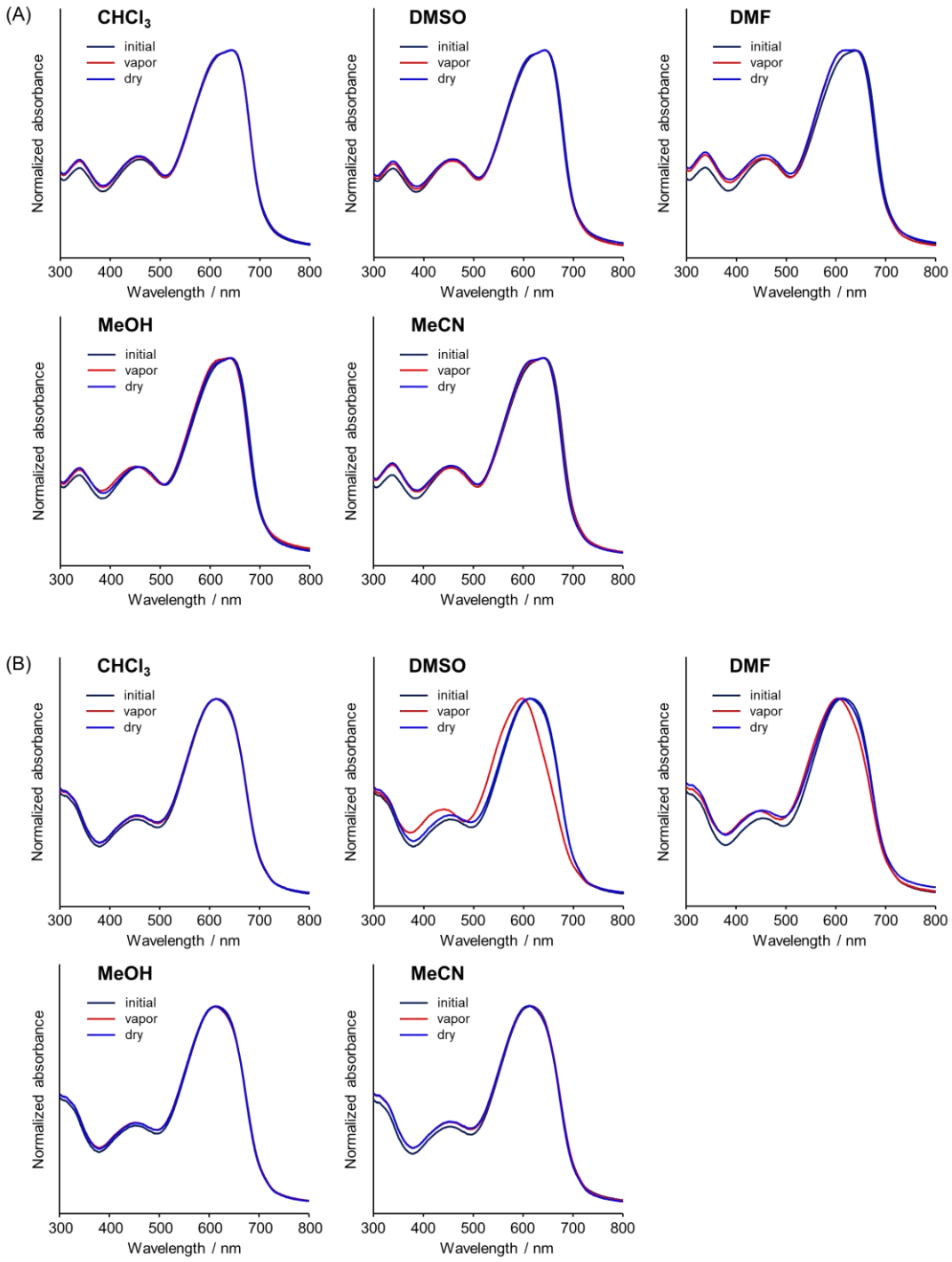

Figure S10. UV–vis absorption spectra of (A) **P-TAzMe** and (B) **P-TAzPh** in film before and after solvent annealing for 30 min, and recovery test by drying the film for 30 min at ambient condition.

PL spectra in film

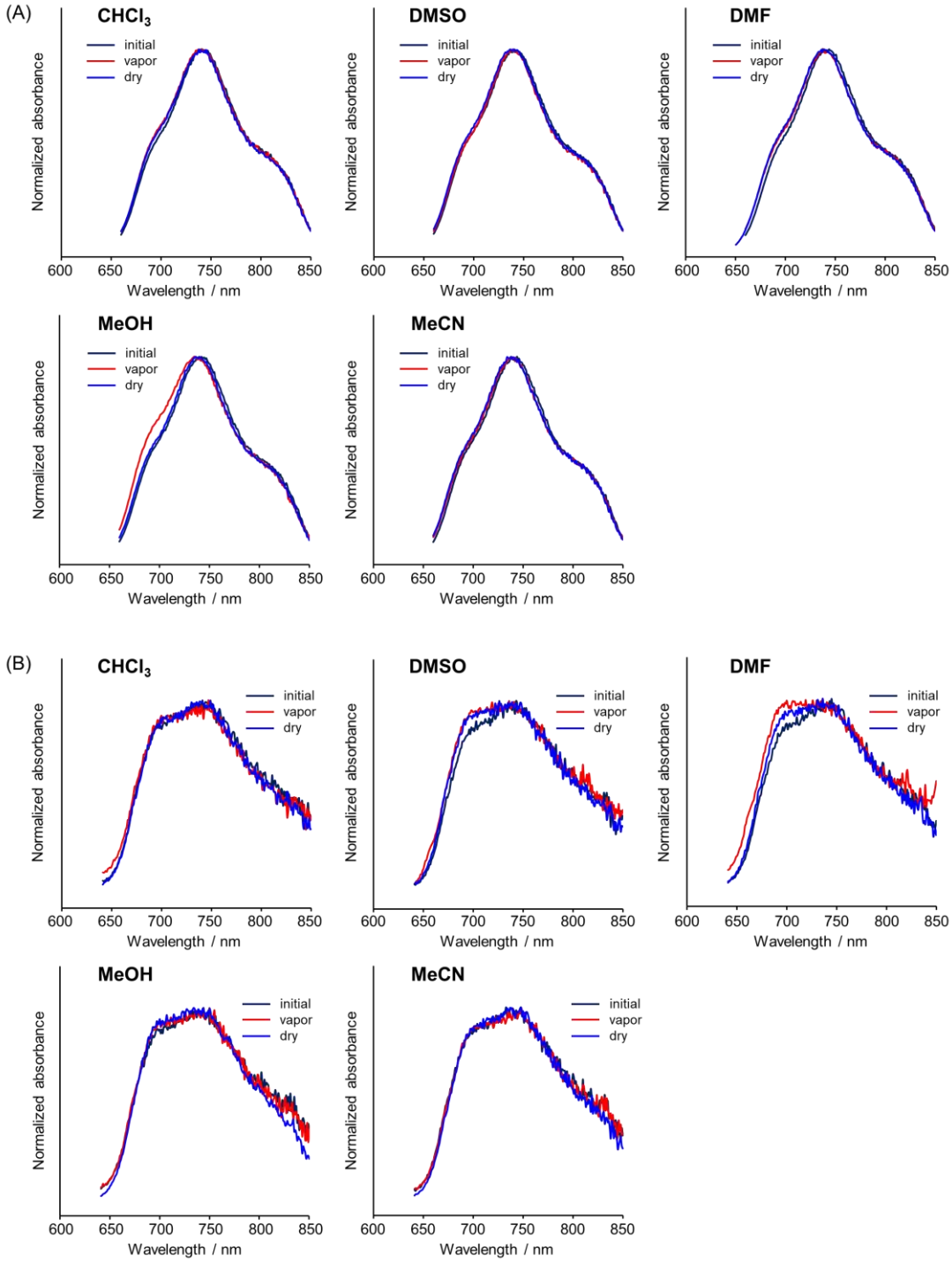

Figure S11. PL spectra of (A) **P-TAzMe** and (B) **P-TAzPh** in film before and after solvent annealing for 30 min, and recovery test by drying the film for 30 min at ambient condition.

Computational details for theoretical calculation

The Gaussian 16 program package[6] was used for computation. We optimized the structures of the **TAzMe**, **TAzPh**, **M-TAzMe** and **M-TAzPh**, and their DMSO adducts **TAzMe-DMSO**, **TAzPh-DMSO**, **M-TAzMe-DMSO** and **M-TAzPh-DMSO** in the ground S_0 states and calculated their molecular orbitals. The DFT was applied for the optimization of the structures in the S_0 states at B3LYP/6-311G(d,p) level for C, H, N, O, Br, S and LanL2DZ for Sn. We calculated the energy of the S_0–S_1 transitions with optimized geometries in the S_0 states by time-dependent (TD) DFT at B3LYP/6-311G(d,p) level for C, H, N, O, Br, S and LanL2DZ for Sn.

Chemical structures

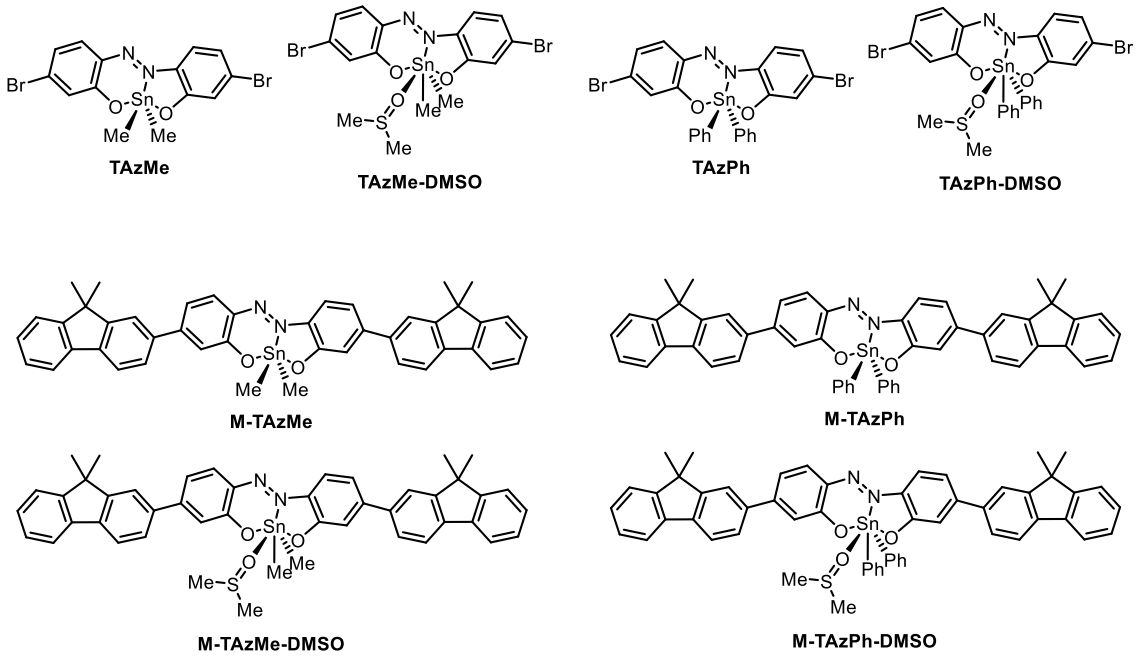

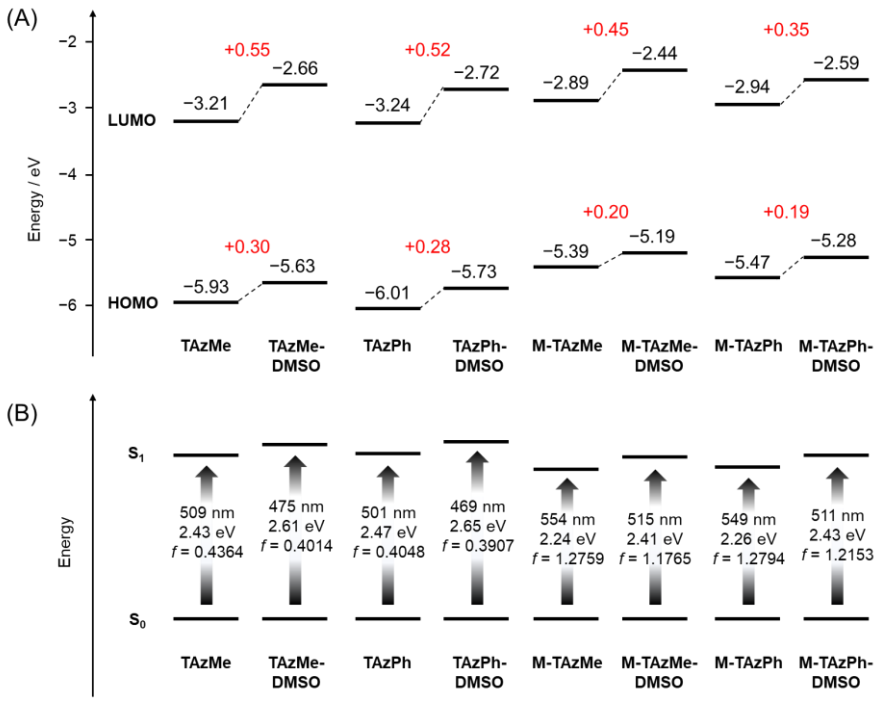

Figure S12. (A) Calculated HOMO and LUMO energy levels, and (B) calculated $S_0 \rightarrow S_1$ transition bands and oscillator strengths (*f*) with DFT and TD-DFT.

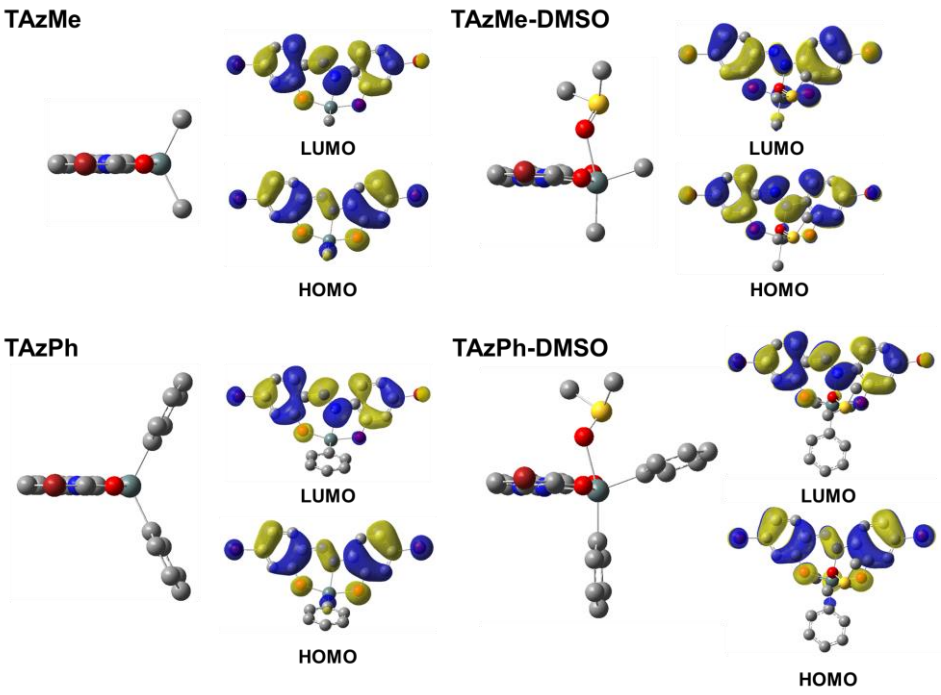

Figure S13. Side view of optimized structures, and selected Kohn–Sham orbitals (isovalue = 0.02) of **TAzMe**, **TAzMe-DMSO**, **TAzPh** and **TAzPh-DMSO**.

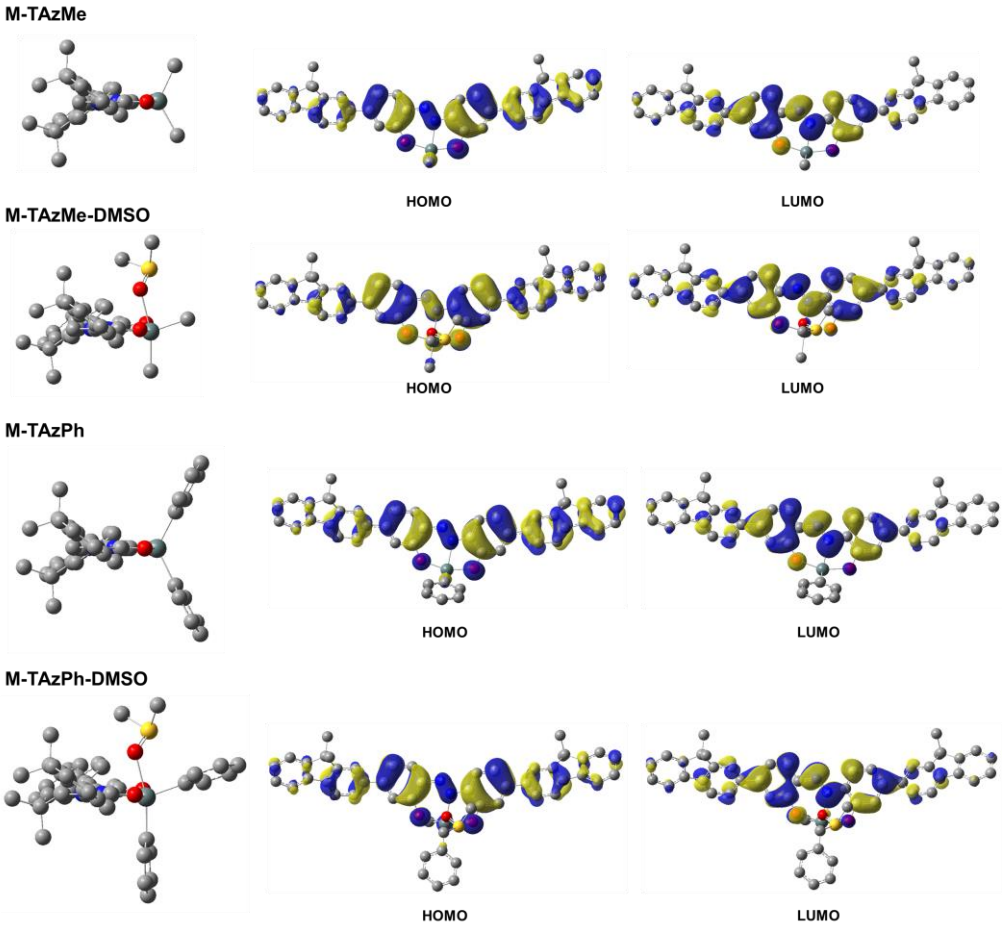

Figure S14. Side view of optimized structures, and selected Kohn–Sham orbitals (isovalue = 0.02) of **M-TAzMe**, **M-TAzMe-DMSO**, **M-TAzPh** and **M-TAzPh-DMSO**.

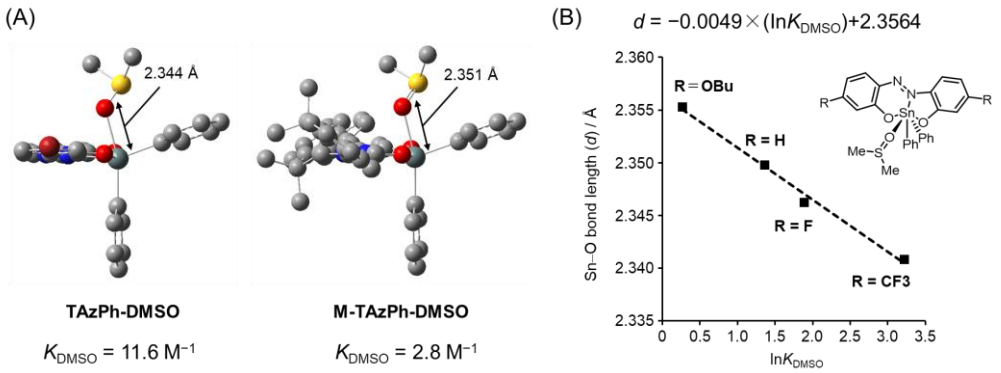

Figure S15. (A) The optimized structures and simulated Sn–O (DMSO) bond lengths of **TAzPh-DMSO** and **M-TAzPh-DMSO** with DFT. (B) The relationship between simulated Sn–O (DMSO) bond lengths of TAz-DMSO compounds and measured binding constants (K_{DMSO}) in toluene at ambient temperature from ref. 5.

References

1. A. B. Pangborn, M. A. Giardello, R. H. Grubbs, R. K. Rosen, F. J. Timmers, Safe and Convenient Procedure for Solvent Purification. *Organometallics*, 1996, **15**, 1518–1520.
2. M. Gon, K. Tanaka and Y. Chujo, A Highly Efficient Near-Infrared-Emissive Copolymer with a N=N Double-Bond π-Conjugated System Based on a Fused Azobenzene-Boron Complex. *Angew. Chem. Int. Ed.*, 2018, **57**, 6546–6551.
3. B. Meng, H. Song, X. Chen, Z. Xie, J. Liu and L. Wang, Replacing Alkyl with Oligo(ethylene glycol) as Side Chains of Conjugated Polymers for Close π–π Stacking. *Macromolecules*, 2015, **48**, 4357–4363.
4. V. Mitchell, W. W. Wong, M. Thelakkat, D. Jones, The synthesis and purification of amphiphilic conjugated donor–acceptor block copolymers. *Polym. J.*, 2017, **49**, 155–161.
5. M. Gon, K. Tanaka and Y. Chujo, Vapochromic Luminescent π-Conjugated Systems with Reversible Coordination-Number Control of Hypervalent Tin(IV)-Fused Azobenzene Complexes. *Chem. Eur. J.*, 2021, **27**, 7561–7571.
6. Gaussian 16, Revision C.01, M. J. Frisch, G. W. Trucks, H. B. Schlegel, G. E. Scuseria, M. A. Robb, J. R. Cheeseman, G. Scalmani, V. Barone, G. A. Petersson, H. Nakatsuji, X. Li, M. Caricato, A. V. Marenich, J. Bloino, B. G. Janesko, R. Gomperts, B. Mennucci, H. P. Hratchian, J. V. Ortiz, A. F. Izmaylov, J. L. Sonnenberg, D. Williams-Young, F. Ding, F. Lipparini, F. Egidi, J. Goings, B. Peng, A. Petrone, T. Henderson, D. Ranasinghe, V. G. Zakrzewski, J. Gao, N. Rega, G. Zheng, W. Liang, M. Hada, M. Ehara, K. Toyota, R. Fukuda, J. Hasegawa, M. Ishida, T. Nakajima, Y. Honda, O. Kitao, H. Nakai, T. Vreven, K. Throssell, J. A. Montgomery, Jr., J. E. Peralta, F. Ogliaro, M. J. Bearpark, J. J. Heyd, E. N. Brothers, K. N. Kudin, V. N. Staroverov, T. A. Keith, R. Kobayashi, J. Normand, K. Raghavachari, A. P. Rendell, J. C. Burant, S. S. Iyengar, J. Tomasi, M. Cossi, J. M. Millam, M. Klene, C. Adamo, R. Cammi, J. W. Ochterski, R. L. Martin, K. Morokuma, O. Farkas, J. B. Foresman and D. J. Fox, Gaussian, Inc., Wallingford CT, 2016.